The role of methyl cycle and N^6-methyladenosine in the regulation of biological clock

2019

YE Shiqi

CONTENTS

PROLEGOMENON

The methyl cycle is a universally conserved metabolic pathway operating in prokaryotes and eukaryotes. In this pathway, S-adenosylmethionine (SAM) is used as the methyl donor co-substrate by many methyltransferases that add methyl groups on various biomolecules such as nucleic acids and histones, which is the foundation of epigenetic regulations of spatiotemporal gene expression. The methyl cycle is indispensable for key cellular functions, and its disruption causes a variety of diseases. Previously, our lab reported that inhibition of the methyl cycle in mammalian cells leads to the lengthening of circadian clock period, suggesting that the methyl cycle may be a central regulator of gene expression and metabolism. Since the methyl cycle and the circadian clock are conserved from bacteria to humans, I decided to investigate whether the regulation of the circadian clock by the methyl cycle is also conserved across evolution. Moreover, I also further characterized the N^6-adenosine methylation (m6A) of mRNA as a putative link between the methyl cycle and the clock in mammals.

In the first chapter, I investigated the conservation of the methyl cycle as a regulator of the circadian clock across species. This study, spanning from cyanobacteria to humans, revealed an extraordinary evolutionary conservation of the link between the methyl cycle and the circadian clock. Moreover, the methyl cycle was also shown to regulate the somite segmentation clock, which is also a transcription-translation negative feedback loop (TTFL)-based timing mechanism orchestrating embryonic development in vertebrates. As mentioned above, the methyl cycle regulates the epigenome and epitranscriptome through the methylation on DNA, RNA and histone. In order to gain insights into the mechanisms involved, the circadian clock in cyanobacteria treated with a specific DNA methylation inhibitor was measured, but

no significant effects was detected on the period, while a global direct MTases inhibitor and known mRNA cap methylation inhibitor, had a more pronounced effect on the period compared to the inhibition of the methyl cycle by 3-Deazaneplanocin A (DZnep). I propose the hypothesis that RNA methyltransferases, which are the oldest MTases, are major conserved mediators between the methyl cycle and the biological clock. Supporting this notion, previous results also revealed that specific inhibition of m6A in mRNA was sufficient to elicit period lengthening in mammals. It is therefore likely that RNA methylation, especially m6A, at least partially contributes to the period lengthening observed across species.

Based on these findings, in Chapter 2, I then focused on uncovering the mechanisms linking m6A and the circadian clock in mammals. The m6A is a prevalent and well-studied RNA modification in mammalian cells that has been implicated to be critical in various biological processes. Three types of enzymes are responsible for maintaining the balance of m6A modification: the "writers", the "erasers" and the "readers", the latter being the effectors of epitranscriptomic regulation. The present study mainly focuses on the cytoplasmic reader YTHDF2, which is the most well-studied m6A reader among the other homologues YTHDF1 and 3. Here, I found that *Ythdf2* knock-down (KD) by RNAi leads to an increased circadian period in mouse cells, and *Ythdf*2 knock-out (KO) by CRISPR-CAS9 in mouse embryonic fibroblasts further confirmed these results. I observed that the stability of major TTFL-clock transcripts increased after *Ythdf2* deletion. Next-generation mRNA sequencing revealed that YTHDF2 targets *Per2, Cipc* and *Rora* mRNAs, coding for essential clock components. I also observed that YTHDF2 localization is dynamic and, under heat shock, relocated mainly from a diffuse cytoplasmic distribution to stress granules. This discovery might provide a clue to further clarify the role of YTHDF2 in the regulation of the circadian clock. Overall, YTHDF2 was confirmed as an important modulator of circadian rhythms.

In Chapter 3, my study delved deeper into how m6A regulates the expression of Casein Kinase 1 Delta (CK1δ), a critical kinase that controls circadian rhythms notably via phosphorylating PER2. Studying CK1δ would help understand the link between m6A and the circadian clock and potentially find a new therapeutic strategy for Familial Advanced Sleep Phase Syndrome (FASPS), a circadian sleep disorder originating from a deficiency in PER2 phosphorylation by CK1δ. Interestingly, two alternatively spliced isoforms of *Ck1δ* were discovered, *Ck1δ1* and *Ck1δ2*, both bearing a highly m6A-methylated site in the 3'-UTR. Using *in vitro*-transcribed mRNA coupled with *in vitro* translation assays, I revealed that m6A is an intrinsic negative regulator of *Ck1δ* translation and stability. Since the *Ck1δ* transcripts are methylated in the 3'-UTR, close to the STOP codon, I further investigated the overall role of the 3'-UTR of *Ck1δ* transcripts and revealed that it acts as a limiting factor for *Ck1δ1* and *Ck1δ2* translation: deletion of the 3'-UTR lead to increased translation of *Ck1δ1* and *Ck1δ2*.

In conclusion, these studies revealed and clarified the role of the methyl cycle in the regulation of the biological clock, demonstrating the extraordinary evolutionary conservation of the link between the methyl cycle and the circadian clock. Focusing on m6A methylation as a potential effector, I identified clock targets of the key m6A reader YTHDF2 that mediates the epitranscriptomic regulation of circadian rhythms. These new insights may lay the foundation in pursuit of novel therapeutics to treat diseases related to biological rhythm disorders.

CHAPTER 1

THE METHYL CYCLE IS A CONSERVED REGULATOR OF BIOLOGICAL CLOCKS

GRAPHICAL ABSTRACT
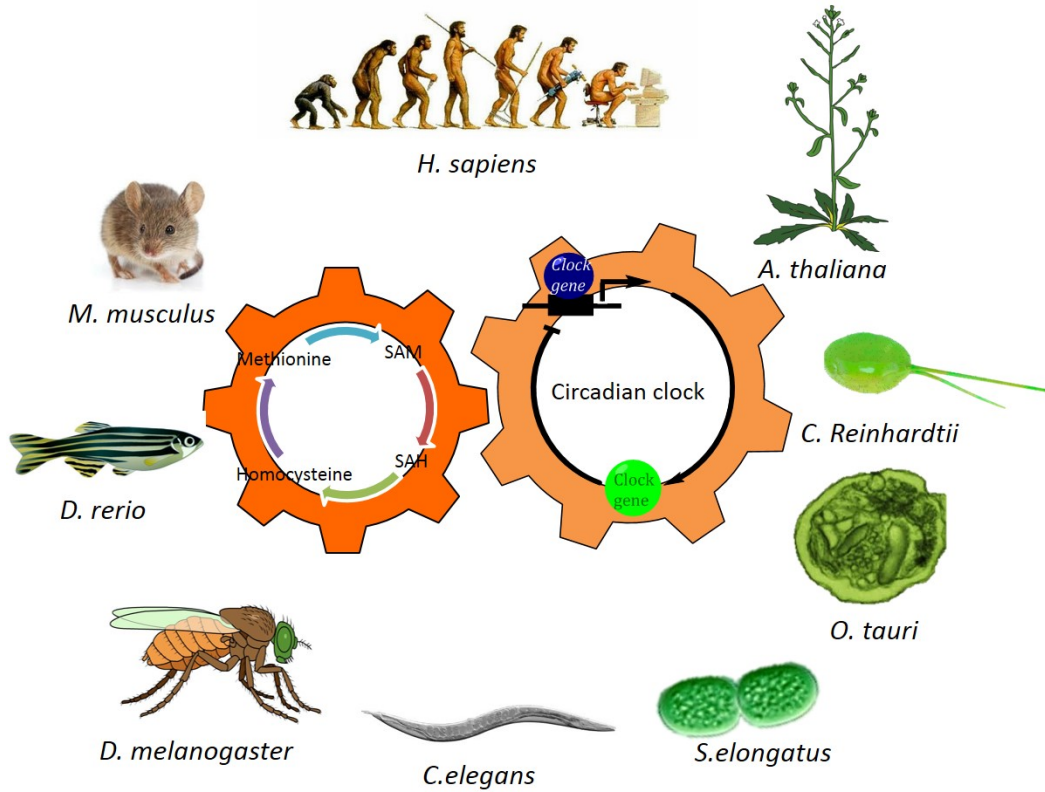
HIGHLIGHTS:

The methyl cycle is a conserved regulator of circadian clocks across species from prokaryotes to mammals.

The methyl cycle also regulates the mouse somite segmentation clock.

THE METHYL CYCLE IS A CONSERVED REGULATOR OF BIOLOGICAL CLOCKS

ABSTRACT

The methyl cycle is a universally conserved metabolic pathway operating in prokaryotes and eukaryotes. In this pathway, the amino acid methionine (Met) is used to synthesize S-adenosylmethionine (SAM), the methyl donor co-substrate in the methylation of nucleic acids, histone and non-histone proteins and many other molecules within the cell. The methylation of nucleic acids and proteins is the foundation of epigenetic and epitranscriptomic regulations of gene expression, but whether the methyl cycle centrally regulates gene expression and function by controlling the availability of methyl moieties is poorly understood.

From cyanobacteria to humans, a circadian clock that involves an exquisitely regulated transcription-translation-feedback loop (TTFL) driving oscillations in gene expression and orchestrating physiology and behavior has been described. It was reported previously that inhibition of the methyl cycle in mammalian cells caused the lengthening of the period of these oscillations, suggesting that the methyl cycle may indeed act as a central regulator of gene expression, at least in mammals. Here, the regulation of methyl cycle on the circadian clock, given their universal presence among living organisms, was investigated in species across the phylogenetic tree of life. A remarkable evolutionary conservation of the link between the methyl cycle and the circadian clock was revealed. Moreover, the methyl cycle regulates the somite segmentation clock, another transcription-translation negative feedback loop-based timing mechanism that orchestrates embryonic development in vertebrates, was also shown, highlighting the methyl cycle as a master regulator of biological clocks.

INTRODUCTION

Methylation reactions start with the metabolization of methionine (Met) into S-adenosylmethionine, or SAM: the universal methyl donor co-substrate in the transmethylation of nucleic acids, proteins, carbohydrates, phospholipids and small molecules. During the methylation process, SAM is converted into adenosylhomocysteine (SAH) that is rapidly hydrolyzed into homocysteine to prevent competitive inhibition of methyltransferase enzymes by SAH due to its close structural relatedness to SAM. Homocysteine is detrimental to physiology [1], and is recycled back into Met or used for glutathione synthesis via cysteine and cystathionine in the trans-sulfidation pathway. The ratio SAM/SAH is known as an indicator of the methylation potential: a measure of the tendency to methylate biomolecules [2-4]. In plants, fungi, prokaryotes and other microorganisms, the methyl cycle is used both as a source of SAM, as well as a source of *de novo* Met synthesis for growth. In a wide variety of eukaryotes, however, Met is an essential amino acid that must be obtained from food, especially in periods of growth, the methyl cycle in these organisms ensuring only the flow of one-carbon units to SAM.

Three enzymatic activities are required to keep the methyl cycle running. 5-Methyl-tetrahydrofolate or betaine is used as a source of methyl moieties to regenerate Met from homocysteine (Hcy). The enzyme *methyltetrahydrofolate-homocysteine S-methyltransferase* is universal but *betaine-Homocysteine methyltransferase* is present only in some vertebrate tissues, mainly in the liver. Likewise, *adenosylmethionine synthetase* (SAM synthesis from Met) and *adenosylhomocysteinase* (AHCY) (Hcy synthesis from SAH) are virtually universal. There is considerable divergence in methyltransferases (MTases), and the phylogeny of five structural classes of MTases is unclear. The oldest MTase represents the RNA methyltransferases, appearing in the early forms of life evolving on Earth in an RNA World [5]. Methyl cycle metabolites are thought to have been present in the prebiotic world, since Met can be created by a spark discharge and is

proposed to be an intermediate in the prebiotic synthesis of homocysteine, which was also found among organic molecules synthesized in the 1972 during Miller experiment [6]. Prebiotic chemistry might have involved methylation by reaction with formaldehyde, an abundant prebiotic organic molecule, to prime the evolution of biological methylation reactions [7].

Similarly, an endogenous circadian clock evolved to anticipate the daily cycles of light and darkness has been found in many organisms, from cyanobacteria to humans. Transcription-translation feedback loops (TTFLs) of "clock genes" directly or indirectly regulating their own transcription underlie many functions of the clock, and drive oscillations of output genes controlling physiology and behavior. Some molecular components of the clock are remarkably conserved in metazoan, notably the genes *Clock* and *Period*, coding for transcription factors, with *Clock* activating the transcription of *Per* and *Per* inhibiting its own transcription.

In 2013, it was reported that disruption of the methyl cycle by inhibitors of AHCY, causing an accumulation of SAH known to lead to a general inhibition of transmethylations, strongly affected the circadian clock in mouse and human cells [8]. Here I show that the link between the methyl cycle and the circadian clock, first uncovered in mammals, has been conserved during more than 2.5 billion years of evolution. A similar link between the methyl cycle and another TTFL called the somite segmentation clock that underlies the development of early body plan in vertebrates was further revealed, indicating that the methyl cycle is a key regulator of biological clocks.

METHODS AND MATERIALS

Molecular modelling and sequence analyses

Crystal protein structures were obtained from the Protein Data Bank (PDB) for *Homo sapiens* (PDB 1LI4 [9], S-adenosylhomocysteine hydrolase complexed with neplanocin, resolution 2.01 Å) and *Mus musculus* (PDB 5AXA [10],

S-adenosylhomocysteine hydrolase with Adenosine, chain A, resolution 1.55 Å). All PDB structures underwent preprocessing including the addition of missing amino acid atoms and hydrogens, removal of solvent atoms, and hydrogen-bond network optimization and residue protonation based on predicted pKa values using the Protein Preparation Wizard [11] of Maestro Schrödinger Release 2018-1 [Maestro, Schrödinger, LLC, New York, NY, 2018]. Homology models of *Danio rerio* (PDB 1LI4, 100 % coverage, 86 % sequence identity), *Drosophila melanogaster* (PDB 1LI4, 100 % coverage, 81 % sequence identity), *Caenorhabditis elegans* (PDB 1LI4, 98 % coverage, 77 % sequence identity), *Arabidopsis thaliana* (PDB 3OND [12] chain A, resolution 1.17 Å, 100 % coverage, sequence 92 % identity), *Chlamydomonas reinhardtii* (PDB 3OND chain A, 100 % coverage, sequence 80 % identity), *Ostreococcus tauri* (PDB 3OND chain A, 99 % coverage, 79 % sequence identity), and *Synechococcus elongatus* (PDB 1LI4, 98 % coverage, 41 % sequence identity) were constructed via the SWISS-MODEL server [13]. Model quality was evaluated based on global model quality estimation (GMQE) ranging from zero to one with high numbers indicating high model reliability, and QMEAN [14], a composite and absolute measure for the quality of protein models, indicating good or poor agreement between model and template with values of around 0 or below -4, respectively. GMQE and QMEAN values for the seven homology models were determined to be 0.98 and 0.85 for *D. rerio*, 0.93 and 0.82 for *D. melanogaster*, 0.87 and 0.35 for *C. elegans*, 0.99 and 0.31 for *A. thaliana*, 0.95 and 0.08 for *C. reinhardtii*, 0.91 and -0.54 for *O. tauri*, and 0.75 and -0.59 for *S. elongatus*, respectively. GROMACS version 2018 [15] was utilized for energy minimization of all nine protein structures including oxidized cofactor NAD^+ using force field AMBERff99SB-ILDN [16]. Cofactor parameters and topologies were obtained through ACPYPE [17] using the AM1-BCC method with net charge *q = -1*. The systems including TIP3P water were neutralized with counter ions (Cl^- and Na^+) to 0.1 M and minimized via steepest descent with a maximum force limit of 100 kJ mol^{-1} nm^{-1}. Molecular docking simulations were performed using the

energy-minimized protein-NAD$^+$ complexes as well as co-crystallized adenosine (ADN), neplanocin (NOC), and 3-deazaneplanocin A (DZnep, constructed from co-crystal NOC in 1LI4 [9] using the Lamarckian Genetic Algorithm provided by the AutoDock4.2 suite [18]. Protein-ligand interactions were analyzed in LigandScout version 4.2 [19].

Multiple sequence alignment of AHCY was performed by CLUSTALW [20] with the multiple sequence viewer from the Maestro module using the following reference sequences: for human, Genbank: NP_000678.1; mouse, Genbank: NP_057870.3; zebrafish, Genbank: NP_954688.1; fruit fly, Genbank: NP_511164.2; C. elegans, Genbank: NP_491955.1; *Arabidopsis*: NP_193130.1; *Chlamydomonas*, Genbank: XP_001693339.1; *Ostreococcus*, Genbank: XP_022839640.1; cyanobacteria, Genbank: WP_011243218.1.

<u>Assay for effect of the inhibition of the methyl cycle on vertebrate circadian clock</u>

Human U2OS cells stably transfected with a *Bmal1*-luciferase reporter vector [21] and mouse PER2::LUC MEFs [22] cell lines were cultivated as previously described [8]. Briefly, cells were seeded into 35 mm dishes (Corning) and allow to grow to confluence in DMEM/F12 medium (Nacalai) containing penicillin/streptomycin/amphotericin (Nacalai). Cells were then shocked by dexamethasone (Sigma-Aldrich) 200 nM for 2 hours, followed by a medium changed including 1 mM luciferine (Nacalai). 35 mm dishes were then transferred to an 8-dishes luminometer-incubator (Kronos Dio, Atto). Photons were counted in bins of 2 min at a frequency of 20 min. DZnep was purchased from Sigma-Aldrich.

The generation of a *per1b*-luciferase cell line from zebrafish PAC2 cells has been previously described [23]. Cells were cultured in Leibovitz's L-15 medium (Gibco) containing 15% fetal bovine serum (Biochrom AG), 50 U/mL penicillin/streptomycin (Gibco), and 50 μg/mL gentamicin (Gibco). Cells were seeded at a density of 50,000-100,000 cells per well in quadruplicate wells of a 96-well plate in medium

supplemented with 0.5 mM beetle luciferin (Promega), and drugs were prepared in water and added at the concentrations indicated in the figures and legends. Plates were sealed with clear adhesive TopSeal (Perkin Elmer, Waltham, MA, USA). Cells were exposed to a 12:12 LD cycle for 7 days and then transferred into DD for at least 3 days. Bioluminescence was monitored on a Packard TopCount NXT scintillation counter (28°C). DZnep was purchased from Sigma-Aldrich. Period and amplitude were estimated by BioDare2 [24].

Assay for effect of the inhibition of the methyl cycle on invertebrate circadian clock

Halteres of two- to seven-day old transgenic *ptim*-TIM-LUC males [25] kept under 12 h: 12 h light:dark cycles (LD) at 25°C were bilaterally dry dissected. Each pair was transferred into one well of a 96 well plate (Topcount, Perkin Elmer) filled with medium containing 80% Schneider's medium (Sigma), 20% inactivated Fetal Bovine Serum (Capricorn) and 1% PenStrep (Sigma). Medium was fortified with 226 μM Luciferin (Biosynth) and supplemented with 10, 100, or 250 μM DZnep A diluted in PBS. Plates were sealed with clear adhesive covers and transferred to a TopCount plate reader (PerkinElmer). Bioluminescence emanating from each well was measured hourly in LD for two days, followed by 5 days of constant darkness (DD) at 25°C as previously described [26]. The *ptim*-TIM-LUC reporter contains the timeless (*tim*) promoter sequences driving rhythmic expression of the *tim* cDNA, which is fused to the firefly luciferase cDNA.

C. elegans strain N2 (Bristol strain, wild-type was provided by the Caenorhabditis Genetics Center, University of Minnesota (cbs.umn.edu/cgc/home). Stocks were maintained on plates with nematode growth medium (NGM) seeded with HB101 *Escherichia coli* strain, under 12-h/12-h LD/CW cycle (400/0 lx and CW (18.5/20°C, Δ = 1.5 ± 0.125°C) environmental cycles. Transgenic animals were generated by microinjection of a *Psur-5:: luc::gfp* construct at 50 or 100 ng/μL with the pRF4 marker (100 ng/μL) [27, 28]. Bioluminescence recordings with nematodes are

described in the SI Appendix (available on bioRxiv; https://doi.org/ 10.1101/653667). Period and amplitude were estimated by BioDare2 [24].

<u>Assay for effect of the inhibition of the methyl cycle on plant and algae circadian clock</u>

Ostreococcus tauri cells transgenically expressing a translational fusion of CCA1 to luciferase from the CCA1 promoter (CCA1-LUC) [29] were grown, imaged, and analysed as described previously [30].

For protoplast isolation and luminescent imaging, plants expressing luciferase from the CCA1 promoter in the Col-0 background (kindly provided by Karen Halliday, University of Edinburgh) were grown in sterile soil under long-day conditions (16 h light/8 h dark) at 22°C under 60-70 µmol m^{-2}s^{-1} white LED tube lights (Impact T8). Protoplasts were isolated from 3-week old leaves as previously described [31]. Protoplasts in a solution of 1 mM D-luciferin (Biosynth AG), 5% fetal bovine serum (Sigma), 50µg/ml ampicillin, 140 mM NaCl, 115 mM CaCl$_2$, 4.6 mM KCl, 1.86 mM MES pH 5.7 and 4.6 mM glucose were added to white, flat-bottomed 96-well plates (Lumitrac, Greiner Bio-one) at a concentration of 2x10^5 cells/ml. DZnep (S7120 Selleckchem) was added to the protoplasts to achieve concentrations of 0, 0.125, 0.25, 0.5 or 1 µM from a 1 mM stock solution (prepared in distilled H$_2$O) to a total volume of 200 µL per well. Plates were sealed with a clear adhesive lid (TopSeal-A, Perkin Elmer). Protoplast luminescence was read by a LB942 Tristar^2 plate reader (Berthold Technologies Ltd) every 50 minutes for 3 seconds per well, and kept under continuous red (630 nm) and blue (470 nm) LED light (5 µmol m^{-2}s^{-1} each) at 19°C.

Chlamydomonas reinhardtii strain CBR carrying a codon-adapted luciferase reporter driven by the *tufA* promoter in the chloroplast genome [32, 33] was used. Culture preparation, bioluminescence monitoring, and data analysis were carried out as described previously [33]. Briefly, 5-day-old algal cultures on HS agar medium were

cut out along with the agar by using a glass tube, and transferred to separate wells of a 96-well microtiter plates. Luciferin (final conc. 200 μM) and various concentrations of DZnep (Sigma) were added to the wells. Algae were synchronized by a single cycle of 12-h darkness/12-h light (30 μmol $m^{-2}s^{-1}$) at 17°C before bioluminescence monitoring using a custom-made luminometer-incubator [34] in DD at 17°C. Period and amplitude were estimated by BioDare2 [24].

Assay for effect of the inhibition of the methyl cycle on prokaryotic circadian clock

Vibrio harveyi luciferase encoded by *luxA* and *luxB* (*luxAB*) genes was used as a luminescence reporter in cyanobacterium *Synechococcus elongatus* PCC 7942. Two cyanobacterial clock-regulated reporter strains, *kaiBCp::luxAB* [35] and *psbAIp::luxAB* [36] were selected for the test, *i.e.* expression of the *luxAB* was under control of the promoters of the central clock genes *kaiBC* and the Class I photosynthetic gene *psbAI*, respectively. *Synechococcus* strains were grown in modified BG11 media [37] supplemented with 40 μg/ml of spectinomycin. The cultures grown on BG11 agar plates for 3 days at 30°C under continuous cool-white illumination (LL) (50 μE/m^2s) were toothpicked onto fresh BG11 agar plates containing 0.015 g/L of L-methionine and different concentrations of 3-deazaneplanocin A hydrochloride (Sigma), sinefungin (Abcam) or EGX[i] (ChemBridge 5790780). After a single 12h dark pulse for synchronization, assay of the *in vivo* luminescence rhythms was performed as described previously [35]. Period and amplitude were estimated by BioDare2 [24].

Measurement of *Hes7* oscillations in the mouse presomitic mesoderm

Presomitic mesoderm (PSM) tissues from three littermate *pHes7-UbLuc* transgenic embryos were embedded in 0.35% LMP-agarose/culture medium (10% FBS-DMEM/F12), in a silicon mold mounted onto a φ35mm-glass bottom dish, and luciferin-containing medium with DZnep or vehicle (MilliQ water) were added.

Time-lapse imaging of PSM was performed with an inverted microscope (Olympus IX81) equipped with an Olympus x10 UPlanApo objective (N.A.: 0.8) and a VersArray cooled-CCD camera. 16-bit images were acquired every 5min with Image-Pro Plus (Media Cybernetics), with 2x2 and 4x4 binning and exposures of 100 ms and 4 m 25 s for DIC and chemiluminescent images, respectively. Raw imaging data were processed and quantified by ImageJ [38]. Period and amplitude were estimated by BioDare2 [24].

RESULTS

<u>AHCY is a remarkably conserved key enzyme in the methyl cycle</u>

The use of carbocyclic adenosine analogues such as DZnep as inhibitors of AHCY was established more than 30 years ago [39-41]. The reaction catalyzed by AHCY is the cleavage of SAH to adenosine and L-homocysteine, DZnep inhibiting this reaction by occupying the adenosine binding site. The AHCY crystal structure of human [42], mouse [10] and yellow lupin (*Lupinus luteus*) [43] complexed with adenosine or analogues have been described, and insights into its catalytic activity have been obtained [44-47]. AHCY has been reported to be one of the most evolutionarily conserved proteins [48], but experimentally-determined structures of AHCY with DZnep remain to be described for most organisms investigated here. A full-length multiple sequence alignment (Fig. S1) and homology modelling of AHCY from human to cyanobacteria (Fig. 1a and Movie S1, available on bioRxiv; https://doi.org/ 10.1101/653667) revealed high sequence and predicted tertiary structure conservation. Amino acids contributing to the DZnep binding site showed at least 88% identity between all eukaryotic AHCY sequences, and 78% between human and bacterial sequences, resulting in the DZnep binding site to be highly similar in all organisms investigated (Fig. 1b, c and Fig. S2). Moreover, amino acids that were reported as crucial for the activity of rat AHCY (His55, Asp130, Glu155, Lys186, Asp190, and Asn191 [47]) are perfectly conserved (Fig. S1). In line with the above,

molecular docking simulations of AHCY with adenosine or DZnep revealed comparable ligand binding conformations and estimated binding free energies for all organisms (Fig. 1d and S2). Together these observations strongly support the use of DZnep as a valid approach to test the effects of methyl cycle inhibition on clocks across phyla.

The circadian clock and methyl cycle are linked in vertebrates

The effects of DZnep on the mammalian clock was first tested in a human osteosarcoma cell line that stably transfected with a luciferase reporter vector for the core clock gene *Bmal1* [21] and in mouse embryonic fibroblasts from PER2::LUC knock-in mice expressing a fusion gene between the endogenous core clock protein PER2 and luciferase [22]. These cells are the gold standard for measuring circadian parameters *in vitro* since they allow the oscillating expression of the genes *Bmal1* or *Per2* to be followed in real-time. In human (Fig. 2a) and mouse (Fig. 2b) cells, DZnep dose-dependently increased the period, up to a maximum of ~40 hours and ~30 hours (all comparisons with control, $p < 0.05$), respectively, with 100 µM DZnep.

DZnep was next tested in a non-mammalian cell type, the zebrafish embryonic PAC2 cell line commonly used for circadian studies, and revealed a potent effect of the drug both on circadian period and amplitude (all comparisons with control, $p < 0.05$, Fig. 2c), as in mammals. Since the circadian clock in these cells is directly light-sensitive and can be entrained by light-dark cycles, whether the entrainment of the cells to light was affected by DZnep before release into constant darkness (DD) was also tested. Indeed, a strong effect on entrainment was observed (Fig. 2c). The gene *Per1b* normally peaks at dawn but was severely blunted and delayed in DZNep-treated cells, even at the lowest concentration of DZnep. In DD, period lengthened dramatically to a peak value of over 40 hours at 10 µM that was slightly lower at 100 µM. To conclude, period and amplitude of circadian oscillations of clock gene expression are strongly affected by DZnep in all three vertebrate cell systems.

The circadian clock and methyl cycle are linked in invertebrates

As models for invertebrates, the fruit fly *Drosophila melanogaster* and the nematode *C. elegans* were selected. Flies have been instrumental in molecular circadian biology, allowing the 2017 Nobel laureates and their co-workers to establish the canonical TTFL model underlying circadian oscillations in metazoan [49-51].

In contrast, *C. elegans* is a relatively new model in circadian biology, the general principles governing its circadian clock remaining largely unidentified [52, 53]. Circadian oscillations in the expression of the *sur-5* gene were described a few years ago and used for the real-time monitoring of the nematode's circadian molecular rhythms by luciferase reporter [28].

As observed in vertebrates, DZnep caused dose-dependent period lengthening in *D. melanogaster* haltere cultures from transgenic luciferase reporter TIM-LUC flies (all comparisons with control, $p < 0.05$, Fig. 3a), and a significant effect of 100 μM DZnep was also observed in freely moving nematodes ($p < 0.05$, Fig. 3b), although period changes in flies were of lesser magnitude than observed in vertebrates. Nevertheless, these results indicate that the link between the circadian clock and the methyl cycle is conserved in invertebrates.

The circadian clock and methyl cycle are linked in plants and algae

Fig. 1a and Fig. S1 show that a plant- and green algae-specific region exists in AHCY, from amino acids 151 to 191, which is involved in the interaction of AHCY with adenosine kinase and cap methyltransferase, and required for nuclear targeting of the enzyme [54, 55]. Despite this insertion, however, the domains for SAH and NAD^+ binding are remarkably conserved.

The most commonly used model organism to study circadian rhythms in land plants is *Arabidopsis thaliana*. Thus, the effects of DZnep on luminescent rhythms reporting the expression of the plant evening gene TOC1 in protoplasts was tested (Fig. 4a),

and extended to aquatic unicellular green algae (Fig. 4b and c). *Ostreococcus tauri* and *Chlamydomonas reinhardtii* represent two different classes of unicellular green algae that have been successfully used in circadian studies and constitute great models to investigate cell-autonomous metabolic processes [29, 56-59]. Increasing concentration of DZnep on *Arabidopsis* and algal cell types were tested and a significant (defined as $p < 0.05$) increase in period length and a decrease in amplitude was observed, as in vertebrates. In conclusion, the effects of DZnep treatment on transcriptional rhythms are also conserved in the plant kingdom. These results are especially significant given unicellular algae and humans are separated by more than 1 billion years of evolution.

The circadian clock and methyl cycle are linked in prokaryotes

Eukaryotic circadian clocks involve a complex TTFL system that requires regulated gene expression at every level from transcriptional to post-translational steps: DNA methylation and the histone code, RNA processing, translation efficiency, phosphorylation and other protein modifications [60]. In contrast, a biochemical oscillator in the cyanobacteria *Synechococcus elongatus* can independently generate a ~24-hour rhythm. Ththeree proteins, Kai-A, -B and -C, form a nanocomplex that regulates two key activities of KaiC: ATPase and autophosphorylation. The result is an autonomous and self-sustained phosphorylation-based oscillator ticking with a period close to 24-hour. In a cellular context, this non-transcriptional oscillator controls transcriptional outputs that in turn add robustness to the biochemical oscillator via TTFLs [61-65].

Like all organisms, cyanobacteria synthesize SAM, required for essential transmethylations. In cyanobacteria a more complex response to DZnep than in other organisms was observed, perhaps due to the presence in these cells of a self-sustained biochemical oscillator that drives the TTFL system. While circadian period lengthened in response to low concentrations of DZnep, the amplitude

increased (Fig. 5a). These observations were confirmed using a different reporter strain of *S. elongatus* (Fig. 5b). Probing the methyl cycle-clock relationship further revealed that intermediate concentrations of the drug caused no significant effects on period but still significantly ($p < 0.05$) increased the amplitude (Fig. S3). At 200 µM however, a dramatic reverse effect on oscillations was seen, the amplitude almost completely collapsing (Fig. S3).

Inhibition of methyltransferases by DZnep depends on the unique activity of AHCY to hydrolyze SAH. Some bacterial proteins, such as Mtn in *E.coli* or Pfu in *Streptococcus pyogenes*, however possess a SAH nucleosidase activity that cleaves SAH to adenine and ribosylhomocysteine [66]. If this pathway for AHCY catabolism is active in *S. elongatus*, acting as a buffer against SAH accumulation, it would explain the blunted period response to DZnep compared to eukaryotes. Indeed, SAH nucleosidases have been identified in at least some *Synechococcus* strains, such as PCC7336 and MED-G69 [67]. To circumvent the potential activity of a SAH nucleosidase in *S. elongatus*, the global methylation inhibitor sinefungin, a natural analogue of SAM that directly binds to and inhibit methyltransferases was used [68]. A known antifungal and antibacterial agent whose activity as such has been shown to depend at least partially on the inhibition of mRNA 5'-cap methylation [69], it was previously used at 10 and 100 µM on the cyanobacteria *Anabaena* to elicit non-lethal methylation-dependent morphological changes [70]. Thus, sinefungin was selected to further probe the link between methyltransferases and the circadian period in *S. elongatus*. In both reporter strains, significant dose-dependent period lengthening ($p < 0.05$) was observed (Fig.5c, d, S3). To contrast with sinefungin, a selective bacterial DNA methyltransferase inhibitor with a different molecular footprint from DZnep or sinefungin, the cyclopentaquinoline carboxylic acid EGX[I] (8-ethoxy-6-nitro-3a, 4, 5, 9b-tetrahydro-3H-cyclopenta[c]quinoline-4-carboxylic acid) was also tested [71] (Fig. S4). Since its published IC_{50} for *E.coli* DNA methyltransferase is 9.7 µM [71], EGX[I] at 5 and 50 µM were used but no any consistent effects on the period has observed, with

only a mild period shortening in *kaiBC*p::luxAB cells at 50 μM (Fig S4). At 100 μM or higher, sinefungin showed some growth inhibition during the experiment, but *Synechococcus* still showed healthy rhythms, suggesting that DNA methylation has no direct effect on circadian period. In contrast, at 100 μM or higher EGX[I] was very toxic to cyanobacteria, causing a dramatic collapse of luciferase intensity, with poor rhythms from which circadian parameters could not be reliably extracted.

Together these data show that the circadian clock in cyanobacteria —separated by 2 billion years of evolution from humans— is sensitive to methylation inhibition. This is especially meaningful considering that the cyanobacterial core clock is a phosphorylation-based biochemical oscillator. This also underlines the fundamental role that methyl metabolism kept in the control of physiology and behavior across evolution. Alternative metabolic pathways branching from the methyl cycle may prevent the accumulation of SAH and make prokaryotes more resistant to methylation inhibition by nutrient deprivation.

The somite segmentation clock and methyl cycle are linked

The results so far have shown that the link between the methyl cycle and the circadian TTFL is conserved. What about other biological timekeepers? While the circadian clock involves a TTFL that oscillates with a period near 24-hour, another TTFL, called the somite segmentation clock, cycles much faster and orchestrates the appearance of new somite from the paraxial mesoderm of the developing embryo in vertebrates (Fig. 6). In mouse, the underlying molecular oscillator is centered on the transcription factor *Hairy and Enhancer of Split 7* (*Hes7*), whose expression oscillates with a period close to 2-hour by negative feedback that also induces oscillations of *Notch* and *Fgf* signaling [72, 73].

Like circadian clock genes, *Hes7* oscillatory expression can be monitored in real-time from transgenic mouse embryo expressing highly destabilized luciferase under the control of the *Hes7* promoter. Testing increasing concentrations of DZnep on these

19

transgenic embryos revealed uncanny similarities with results seen so far: an increase in period length (2.5 h increased to 3.2 h, $p < 0.05$) accompanied by a decrease in amplitude of *Hes7* oscillations (18 counts decreased to less than 5 counts, $p < 0.01$) (Fig. 6). This once more illustrates the importance of the methyl cycle in the regulation of transcriptional programs orchestrating development, physiology and behavior.

Here an evidence for the existence of an ancient link between the methyl cycle and biological timekeepers was provided. In the course of more than 2 billion years of cellular evolution, during which the biological clock and the methyl cycle have adapted to a multicellular eukaryotic existence, the link between these two processes has remained active. Further investigations should reveal how the link itself has evolved, and which methylated substrates and methyltransferases are critical for its function.

DISCUSSION

Solar ultraviolet irradiation plays a critical role in prebiotic chemistry and has been involved in the origin of chirality [74], the synthesis of alcohols, aldehydes (notably formaldehyde), and organic acids [75], as well as that of amino acids [76] and ribonucleotides [77]. The presence of methylation transfer in the prebiotic world probably caused the incorporation of methyl chemistry in early life-forms. The energy of UV photons however can also degrade biologically important molecules, preventing abiogenesis. Once autocatalytic pseudo-life forms evolved with more complex chemistry, avoidance mechanisms may have provided increased fitness in such an environment. The origin of the circadian clock on the early earth is likely to have been a simple sensing of molecules present in the milieu, increasing or decreasing under UV exposure and triggering an appropriate response. Formaldehyde, increasing during the day under the action of UV on carbon monoxide and water vapor [76], could have been such a chemical marker of daylight,

affecting the chemistry of early life-forms by methylation. A conserved link between methyl transfer and the circadian clock may have arisen from such a scenario.

The most surprising data obtained here is the almost identical response of unicellular algae and vertebrates to DZnep despite their evolutionary divergence more than 1 billion years ago, the comparable effect of methylation inhibitors on cyanobacterial circadian clock (2 billion years of evolutionary divergence), and the conservation of this biochemical link in the control of the somite segmentation clock. So far, only a small number of examples have been reported that identified aspects of circadian timekeeping shared among rhythmic life, such as oxidation cycles of peroxiredoxin [58, 78, 79] and regulation by oscillating intracellular magnesium concentrations [30].

In mammalian cells, our lab previously reported that methyl cycle inhibition decreased the methylation of internal adenosines in mRNA (m6A), as well as that of histones [8]. While specific m6A inhibition was sufficient to elicit period elongation, the contribution of histone methylation to the period elongation obtained by DZnep was likely significant, as well as that of other methylation sites in mRNA, rRNA and tRNA. Due to the considerable heterogeneity in mechanisms regulating gene expression and function in organisms tested here, identifying a single mechanism explaining period elongation would be a difficult undertaking and is beyond the scope of the present work. The oldest MTases are RNA methyltransferases has mentioned in the introduction [5], it is therefore tempting to propose that inhibition of RNA methylation may at least partially contribute to the period lengthening. This hypothesis is further supported by the fact that sinefungin, a confirmed mRNA cap-methyltransferase inhibitor [69], was able to lengthen the cyanobacterial clock period, but EGX[i], a DNA methylation inhibitor, was not. Although it is also possible that the effects of methyl cycle inhibition on period and amplitude in eukaryotes arise from different mechanisms, e. g. on the inhibition of mRNA and histone methylation, respectively. More experiments should clarify these points.

The presence of a SAH nucleosidase in *S. elongatus* may have blunted the effect of DZnep, but even with 100 µM sinefungin the period lengthened only about 2 hours. It should be mentioned that the luciferase reporter system used is a reporter for the driven TTFL, not for the Kai A, B and C oscillator *per se*. It is therefore possible that methylation inhibition only affected the coupling between the nanocomplex and the TTFL, which may explain why the increase in period was less pronounced compared to most eukaryotes tested here. In eukaryotic cells, luciferase reporter systems are a direct read-out of the core oscillator that has evolved more dependent on the TTFL, and as a result may have become more sensitive to perturbations affecting gene expression such as inhibition of RNA and histone methylation.

The somite segmentation clock was strongly affected by inhibition of AHCY, which is in line with the importance of one carbon metabolism for embryonic development. As can be seen in the Movie S3 (available on bioRxiv; https://doi.org/ 10.1101/653667), showing similar results to Movie S2 (available on bioRxiv; https://doi.org/ 10.1101/653667) but merged with bright field images and displaying luminescence as a pseudo-color green, period lengthening of the oscillatory expression of *Hes7-luciferase* occurred together with a pronounced delay in the growth of the caudal tip of the presomitic mesoderm as well as in the appearance of new somites, demonstrating that the molecular clock as well as its output, *i.e.* the somitogenesis, were affected by DZnep. The mechanisms underlying this period lengthening may be distinct from those involved in the lengthening of the circadian period. Considering the short period of *Hes7* oscillations of around 2h, and the importance of 3'-UTR-dependent regulation of *Hes7* mRNA turnover for its cyclic expression [80], the inhibition of mRNA methylation may at least in part contribute to the results observed.

Despite being one of the most potent AHCY inhibitors [41], DZnep is sometimes erroneously sold and used as a "specific" histone methyltransferase EZH2 inhibitor because of the misinterpretation of a report showing that it inhibits —without any

data on specificity— histone methylation by EZH2 in cancer cells [81]. More recent reports showed that, in line with its inhibitory effect on AHCY [82, 83], DZnep globally inhibits histone methylation.

Since the purpose is to inhibit the methyl cycle in organisms from bacteria to humans, these investigations were by necessity limited to the pharmacological inhibition of AHCY, because irreversible genetic disruption of AHCY in all organisms would have been much less feasible, notably due to likely embryonic lethality or developmental arrest in metazoan, cell cycle/growth disruption, and the existence of multiple uncharacterized homologues in many organisms tested here. This work puts the spotlight on the methyl cycle and calls for more investigations into how it regulates physiology and behavior.
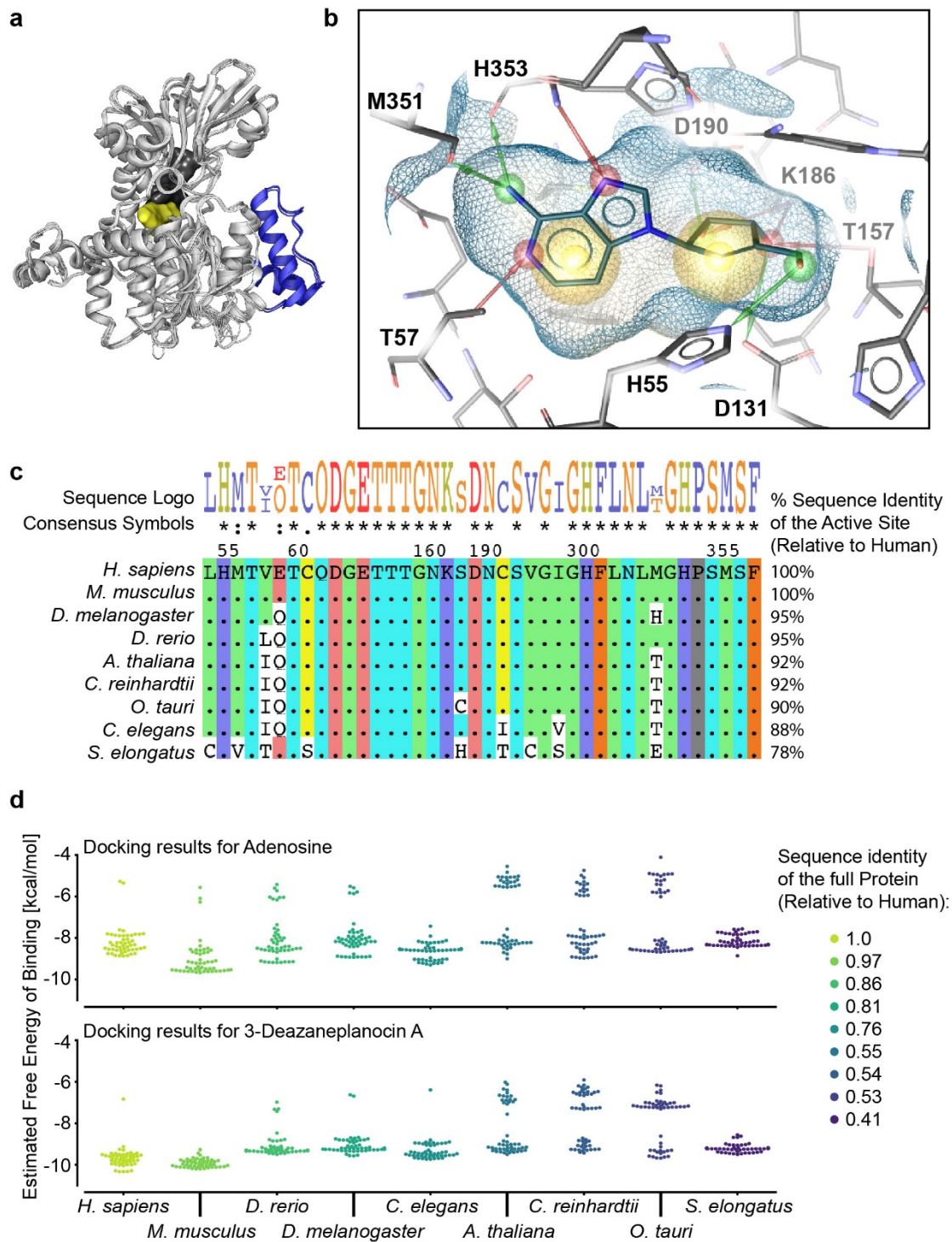
Figure 1. Adenosylhomocysteinase is a highly conserved protein. (a) Structural superposition of AHCY from the 9 organisms investigated here, using human (1LI4), mouse (5AXA) or lupin (3OND) crystal structures as templates. The blue loop is specific to plants and green algae; DZnep is shown in yellow, NAD$^+$ in grey. See also Movie S1 (available on bioRxiv; https://doi.org/ 10.1101/653667). (b) Docking simulation of human AHCY with DZnep, based on the 1LI4 crystal structure of human AHCY complexed with Neplanocin A, an analogue of DZnep. The amino acids

involved in DZnep binding are indicated with their position. See Fig. S2 for docking simulations of DZnep to AHCY from other organisms. Red and green arrows are hydrogen bonds, yellow spheres are hydrophobic effects. The estimated free energy of binding for depicted DZnep docking conformation was -9.87 kcal/mol. (**c**) Discontinuous alignment of amino acids contributing to the binding of DZnep, using the human sequence as a reference and with sequence identities shown on the right. When amino acids are identical to human, a dot is shown in the alignment. The sequence logo on top is a graphical representation of the conservation of amino acids, with the consensus symbols below (* = fully conserved residue, : = conservation of strongly similar properties, . = conservation of weakly similar properties). The positions of selected conserved amino acids are given for the human sequence. (d) Molecular docking simulations of AHCY with adenosine (top) or DZnep (below) showing comparable binding free energies in all organisms. Colors represent full sequence identities, relative to human.
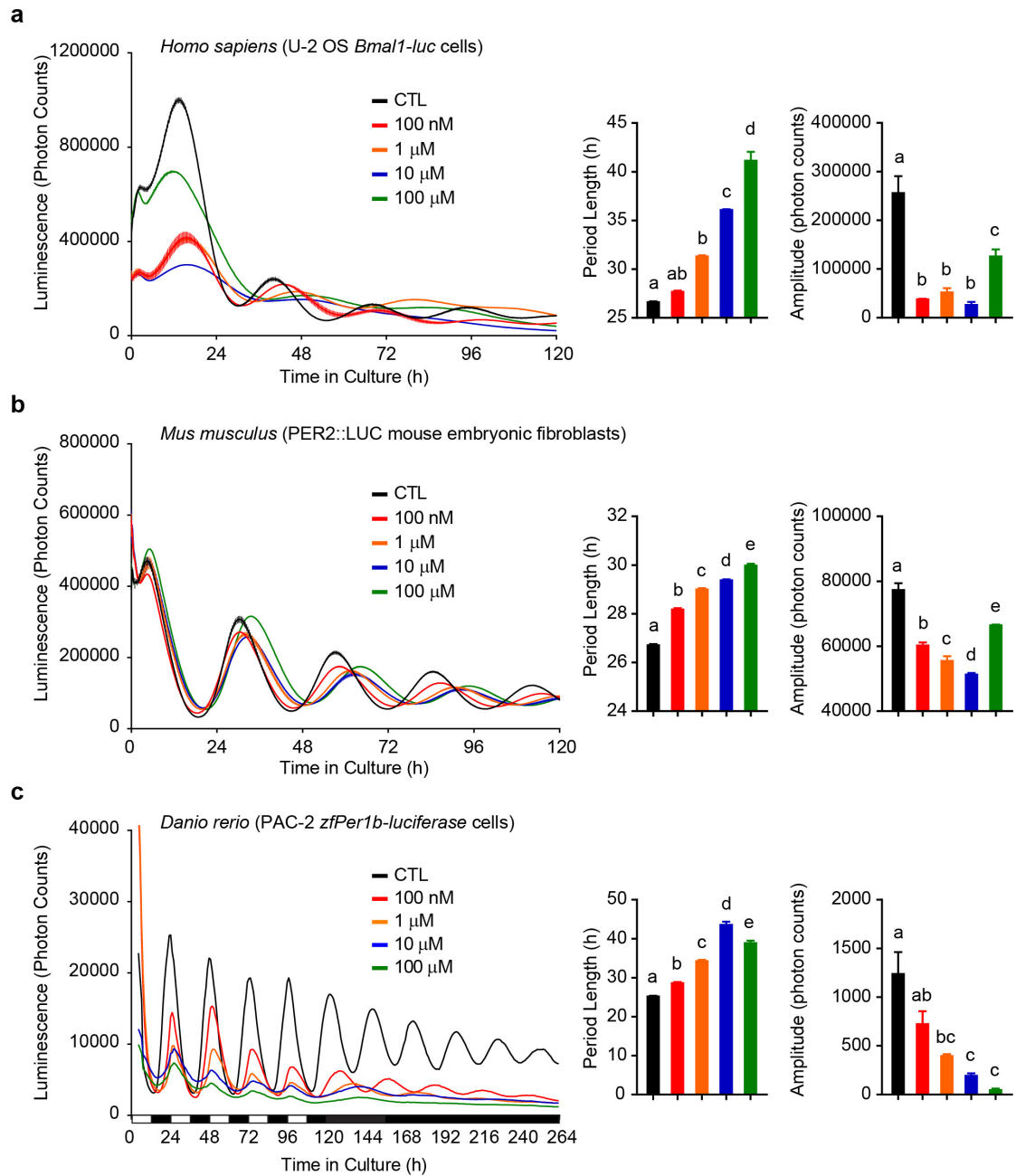
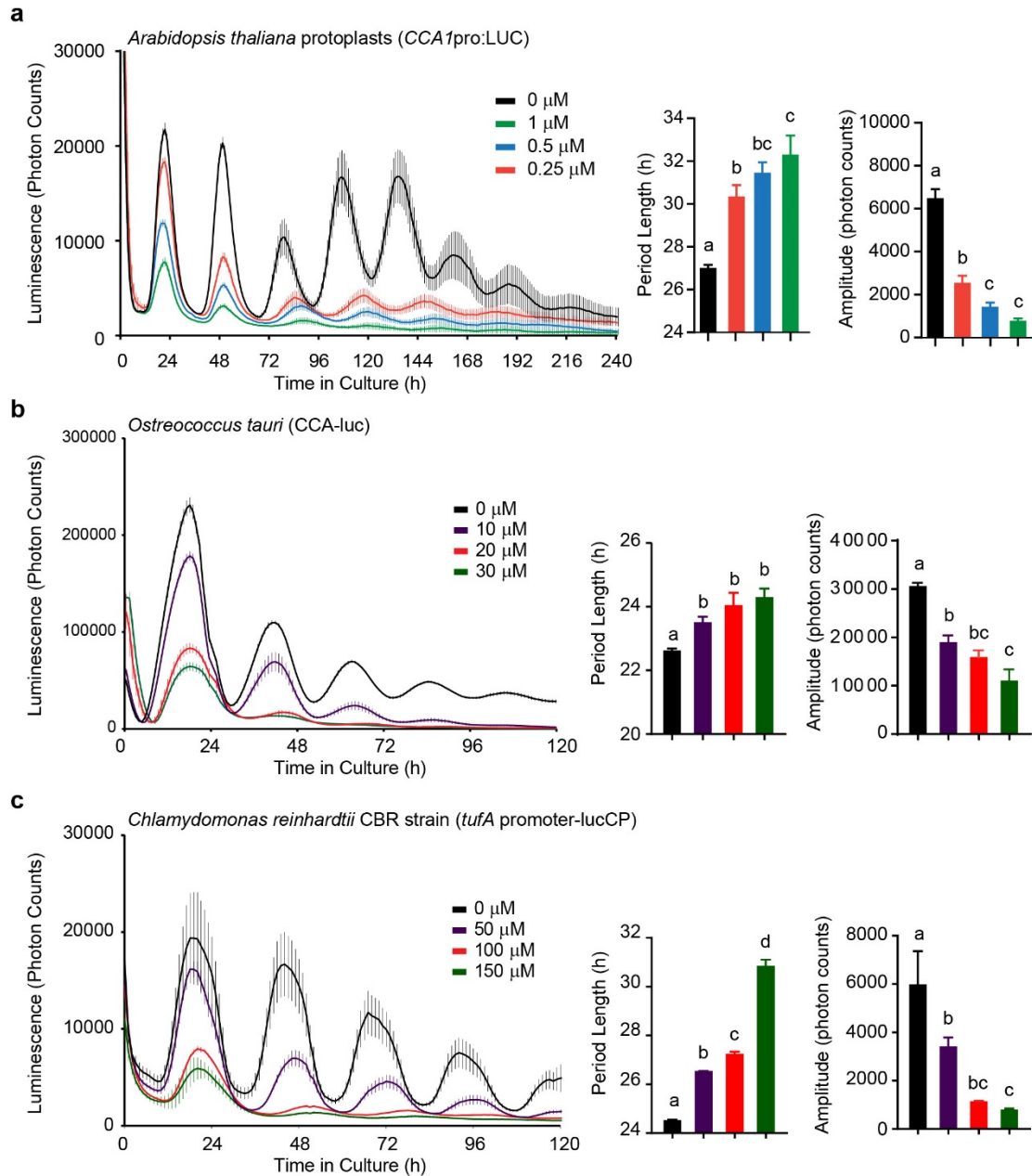**Figure 2. The link between the methyl cycle and the clock is conserved in vertebrates.** (**a**) Left panel shows mean luminescence +/- SEM of human U2OS cells stably transfected by a *Bmal1*-luc reporter and treated with increasing concentrations of DZnep. Middle panel shows mean +/- SEM of period, n = 3. Right panel shows mean +/- SEM of amplitude, n = 3 dishes. Same analyses were performed with PER2::LUC mouse embryonic fibroblasts, n = 3 dishes (**b**), and PAC-2 zebrafish cells stably transfected with a *Per1b*-luciferase reporter, n = 4 dishes, mean +/- SEM (**c**). These experiments were independently reproduced at least three times. All bar graphs analyzed by One-Way ANOVA followed by Bonferroni post-hoc test; *a vs. b vs. c vs. d vs. e*, indicating at least $p < 0.05$ significance.
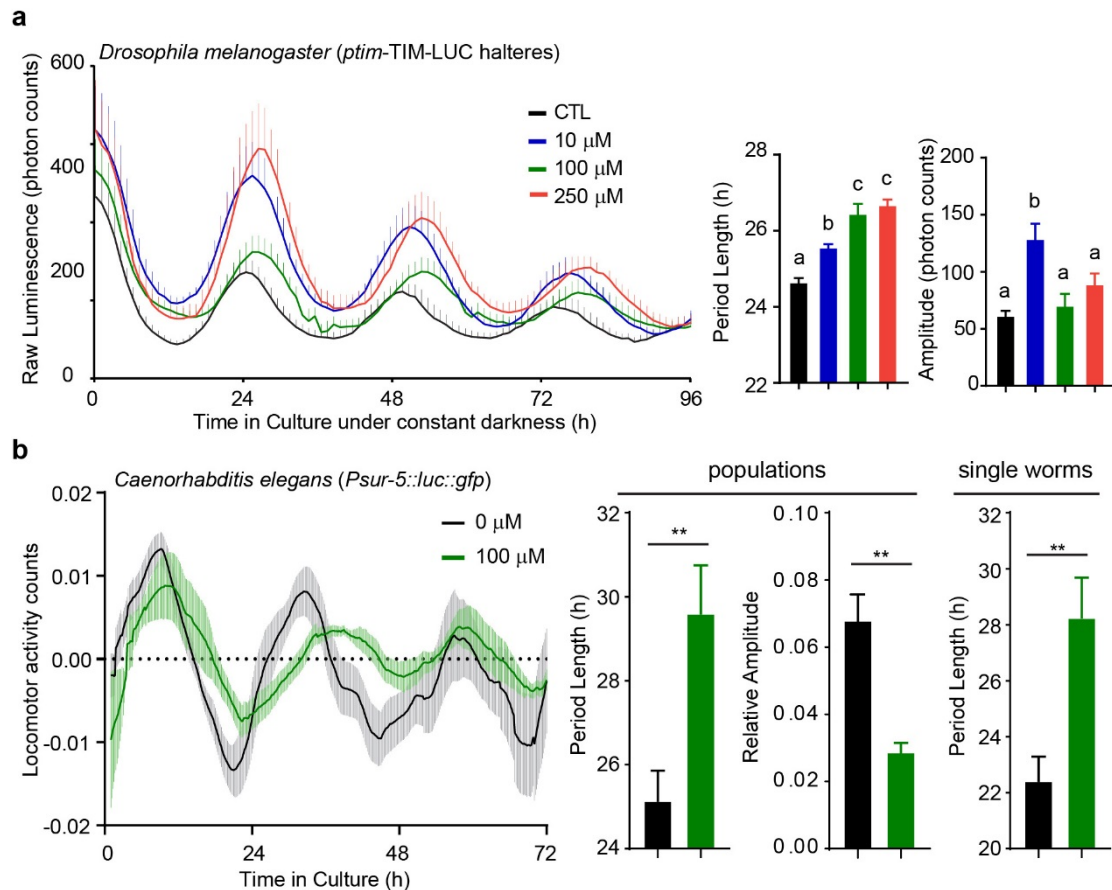
Figure 3. The link between the methyl cycle and the clock is conserved in invertebrates. (*a*) Real-time luminescence from halteres in culture dissected from *ptim*-TIM-LUC male flies. Luminescence traces show mean +/- SEM of n = 8 halteres, with only the upper segment of the error bars shown for clarity. Middle and right panel shows mean +/- SEM of period and amplitude, respectively, for n = at least 8 halteres for each treatment group. All bar graphs analyzed by One-Way ANOVA followed by Bonferroni post-hoc test; *a vs. b vs. c*, indicating at least *p* <0.05 significance. (*b*) Locomotor activity counts from detrended luminescence measurements of freely moving *Caenorhabditis elegans* populations of ~100 nematodes treated with vehicle or 100 µM DZnep, showing mean +/- SEM of n = 10 populations. In the middle, population mean +/- SEM of period (left) and amplitude (right) compared by Student *t*-test; **, *p* < 0.01; n = 10 populations treated with vehicle and n = 6 treated with DZnep. The right panel shows mean +/- SEM of period obtained from single nematodes in isolation, n = 21 controls and 22 for DZnep, analyzed by Student *t*-test, **, *p* < 0.01.

Figure 4. The link between the methyl cycle and the clock is conserved in plants. (a) Left panel shows mean luminescence +/- SEM of *Arabidopsis thaliana* protoplasts bearing a *CCA1pro:*LUC reporter construct, n = 8 wells per treatment, treated with different concentration of DZnep. For comparison between different runs, traces were aligned in relation to the first peak. Middle panel shows mean +/- SEM of amplitude, n = 8. Right panel shows mean +/- SEM of amplitude, n = 8.   **(b)** Same as (a) but with *Ostreococcus tauri* cells carrying a CCA1-LUC reporter, n = 8 wells. Middle panel shows mean +/- SEM of period, n = 8 wells. No significance was observed between 10, 20 and 30 µM, but the significance compared to 0 µM became stronger, *i.e. p* < 0.05, *p* < 0.001, *p* < 0.0001, respectively, indicating dose-dependent effects. Right panel shows mean +/- SEM of amplitude, n = 8 wells. **(c)** Same as (b)

but with *Chlamydomonas reinhardtii* CBR strain cultures stably-transfected with a *tufA* promoter-lucCP reporter, n = 5 wells. Middle panel shows mean +/- SEM of period, n = 5 wells. Right panel shows mean +/- SEM of amplitude, n =5 wells. All bar graphs analyzed by One-Way ANOVA followed by Bonferroni post-hoc test; *a vs. b vs. c*, indicating at least p <0.05 significance.
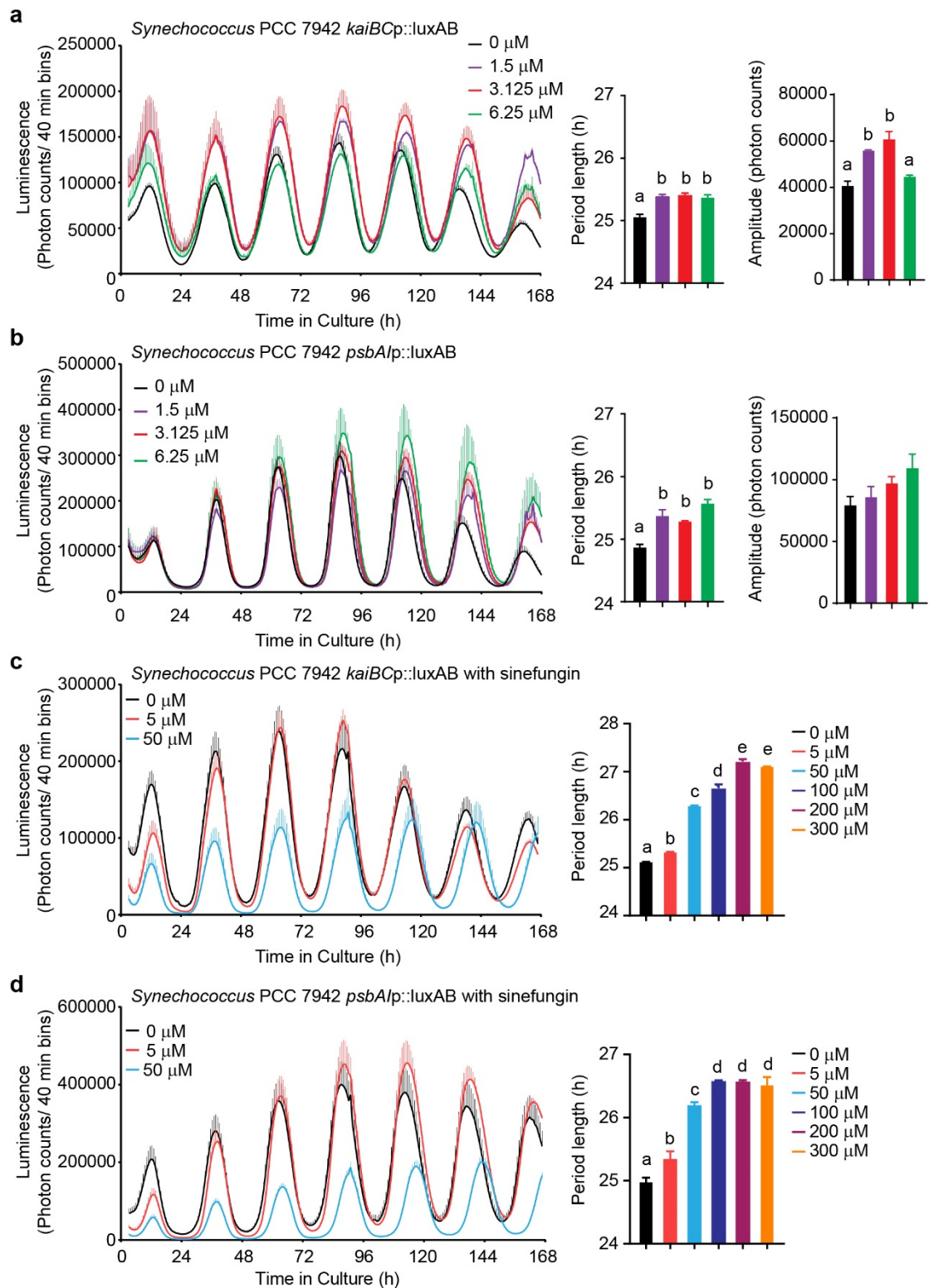
Figure 5. The link between the methyl cycle and the clock is conserved in cyanobacteria. (**a**) Left panel shows mean luminescence +/- SEM of *Synechococcus* PCC 7942 *kaiBC*p::luxAB knock-in strain treated with different concentrations of DZnep, n = 3, with only the upper section of the error bars shown for clarity. Middle panel shows mean period +/- SEM, n = 3. Right panel shows mean amplitude +/- SEM, n = 3. (**b**) Same as (a) but using *Synechococcus* PCC 7942 *psbAI*p::luxAB knock-in

strain. Data for (a) and (b) were analyzed together with data from Fig. S3, showing additional concentrations of DZnep. (**c**) and (**d**) are the same as (a) and (b), respectively, but with different sinefungin concentrations as indicated over the graphs. In addition, bar charts in (c) and (d) show data obtained with higher concentrations of sinefungin presented in Fig. S3. See also Fig. S4 for a comparison with EGX[I]. All bar graphs analyzed by One-Way ANOVA followed by Bonferroni post-hoc test; *a vs. b vs. c vs. d vs. e*, indicating at least $p < 0.05$ significance.
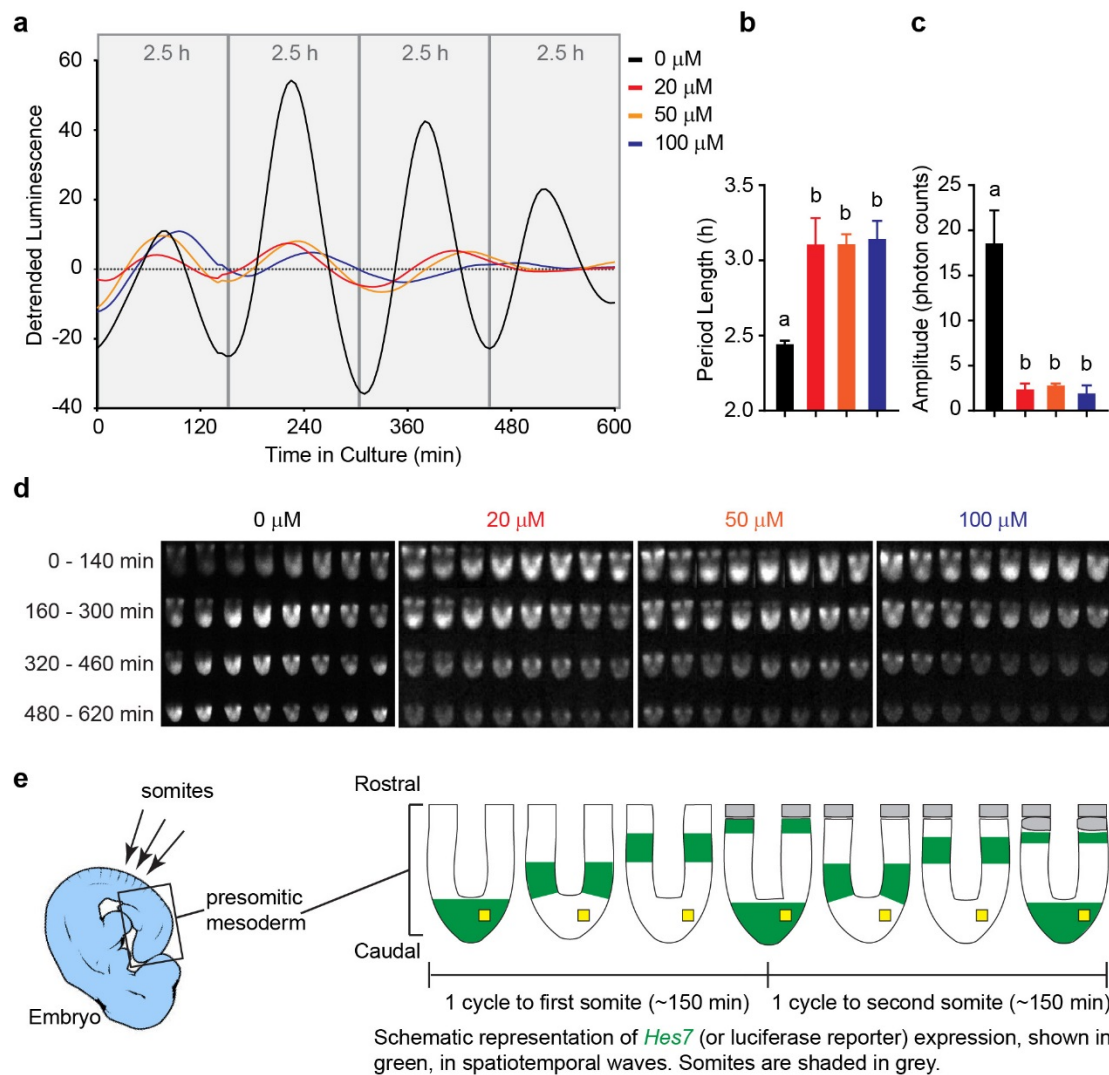
Figure 6. The somite segmentation clock is sensitive to methyl cycle inhibition. (a) Representative detrended luminescence measurements from one cultured embryo per treatment as indicated in the legend on the right. (**b**) Mean period +/- SEM of n = 3 embryos per treatment, with *a vs. b*, indicating *p* <0.05 significance. (**c**) Mean amplitude +/- SEM of n = 3 embryos per treatment, with *a vs. b*, indicating *p* <0.05 significance. (**d**) Montage of luminescence time-lapse micrographs of one representative embryo for each treatment. One picture every 20 min is shown, starting from top left, each row corresponding to one Hes7 expression cycle in the embryo treated with 0 μM DZnep, as shown in (a). See also Movies S2 and S3 (available on bioRxiv; https://doi.org/ 10.1101/653667). (**e**) Anatomic localization of the presomitic mesoderm in embryo and schematic representation of the pictures from (d). The yellow square defined the area from which luminescence was measured in (a).

REFERENCES

[1] G. Lippi, M. Plebani. Hyperhomocysteinemia in health and disease: where we are now, and where do we go from here? Clin Chem Lab Med, 50 (2012) 2075-2080.

[2] G.L. Cantoni. The role of S-adenosylhomocysteine in the biological utilization of S-adenosylmethionine. Prog Clin Biol Res, 198 (1985) 47-65.

[3] P.K. Chiang, G.L. Cantoni. Perturbation of biochemical transmethylations by 3-deazaadenosine in vivo. Biochem Pharmacol, 28 (1979) 1897-1902.

[4] D.R. Hoffman, D.W. Marion, W.E. Cornatzer, J.A. Duerre. S-Adenosylmethionine and S-adenosylhomocystein metabolism in isolated rat liver. Effects of L-methionine, L-homocystein, and adenosine. J Biol Chem, 255 (1980) 10822-10827.

[5] A.K. Rana, S. Ankri. Reviving the RNA world: an insight into the appearance of RNA methyltransferases. Front Genet, 7 (2016) 99.

[6] J.E. Van Trump, S.L. Miller. Prebiotic synthesis of methionine. Science, 178 (1972) 859-860.

[7] T.G. Waddell, L.L. Eilders, B.P. Patel, M. Sims. Prebiotic methylation and the evolution of methyl transfer reactions in living cells. Orig Life Evol Biosph, 30 (2000) 539-548.

[8] J.M. Fustin, M. Doi, Y. Yamaguchi, H. Hida, S. Nishimura, M. Yoshida, . . . H. Okamura. RNA-methylation-dependent RNA processing controls the speed of the circadian clock. Cell, 155 (2013) 793-806.

[9] X. Yang, Y. Hu, D.H. Yin, M.A. Turner, M. Wang, R.T. Borchardt, . . . R.L. Schowen. Catalytic Strategy of S-Adenosyl-l-homocysteine Hydrolase: Transition-State Stabilization and the Avoidance of Abortive Reactions. Biochemistry, 42 (2003) 1900-1909.

[10] Y. Kusakabe, M. Ishihara, T. Umeda, D. Kuroda, M. Nakanishi, Y. Kitade, . . . N. Tanaka. Structural insights into the reaction mechanism of S-adenosyl-L-homocysteine hydrolase. Sci Rep, 5 (2015) 16641.

[11] G.M. Sastry, M. Adzhigirey, T. Day, R. Annabhimoju, W. Sherman. Protein and ligand preparation: parameters, protocols, and influence on virtual screening enrichments. J Comput Aided Mol Des, 27 (2013) 221-234.

[12] K. Brzezinski, Z. Dauter, M. Jaskolski. High-resolution structures of complexes of plant S-adenosyl-L-homocysteine hydrolase (Lupinus luteus). Acta Crystallogr D Biol Crystallogr, 68 (2012) 218-231.

[13] A. Waterhouse, M. Bertoni, S. Bienert, G. Studer, G. Tauriello, R. Gumienny, . . . T. Schwede. SWISS-MODEL: homology modelling of protein structures and complexes. Nucleic Acids Res, 46 (2018) 296-303.

[14] P. Benkert, M. Biasini, T. Schwede. Toward the estimation of the absolute quality of individual protein structure models. Bioinformatics, 27 (2011) 343-350.

[15] D. Van Der Spoel, E. Lindahl, B. Hess, G. Groenhof, A.E. Mark, H.J. Berendsen. GROMACS: fast, flexible, and free. J Comput Chem, 26 (2005) 1701-1718.

[16] K. Lindorff-Larsen, S. Piana, K. Palmo, P. Maragakis, J.L. Klepeis, R.O. Dror, D.E. Shaw. Improved side-chain torsion potentials for the Amber ff99SB protein force field. Proteins, 78 (2010) 1950-1958.

[17] A.W. Sousa da Silva, W.F. Vranken. ACPYPE - AnteChamber PYthon Parser interfacE. BMC Res Notes, 5 (2012) 367.

[18] G.M. Morris, R. Huey, W. Lindstrom, M.F. Sanner, R.K. Belew, D.S. Goodsell, A.J. Olson. AutoDock4 and AutoDockTools4: Automated docking with selective receptor flexibility. J Comput Chem, 30 (2009) 2785-2791.

[19] G. Wolber, T. Langer. LigandScout: 3-D pharmacophores derived from protein-bound ligands and their use as virtual screening filters. J Chem Inf Model, 45 (2005) 160-169.

[20] M.A. Larkin, G. Blackshields, N.P. Brown, R. Chenna, P.A. McGettigan, H. McWilliam, . . . D.G. Higgins. Clustal W and Clustal X version 2.0. Bioinformatics, 23 (2007) 2947-2948.

[21] J.E. Baggs, T.S. Price, L. DiTacchio, S. Panda, G.A. Fitzgerald, J.B. Hogenesch. Network features of the mammalian circadian clock. PLoS Biol, 7 (2009) e52.

[22] S.H. Yoo, S. Yamazaki, P.L. Lowrey, K. Shimomura, C.H. Ko, E.D. Buhr, . . . J.S. Takahashi. PERIOD2::LUCIFERASE real-time reporting of circadian dynamics reveals persistent circadian oscillations in mouse peripheral tissues. Proc Natl Acad Sci U S A, 101 (2004) 5339-5346.

[23] D. Vallone, S.B. Gondi, D. Whitmore, N.S. Foulkes. E-box function in a period gene repressed by light. Proc Natl Acad Sci U S A, 101 (2004) 4106-4111.

[24] T. Zielinski, A.M. Moore, E. Troup, K.J. Halliday, A.J. Millar. Strengths and limitations of period estimation methods for circadian data. PloS one, 9 (2014) e96462.

[25] P. Lamba, L.E. Foley, P. Emery. Neural network interactions modulate CRY-dependent photoresponses in Drosophila. J Neurosci, 38 (2018) 6161-6171.

[26] C. Chen, M. Xu, Y. Anantaprakorn, M. Rosing, R. Stanewsky. nocte is required for integrating light and temperature inputs in circadian clock neurons of Drosophila. Curr Biol, 28 (2018) 1595-1605.

[27] C.C. Mello, J.M. Kramer, D. Stinchcomb, V. Ambros. Efficient gene transfer in C.elegans: extrachromosomal maintenance and integration of transforming sequences. Embo J, 10 (1991) 3959-3970.

[28] M.E. Goyaa, A. Romanowski, C.S. Caldart, C.Y. Benard, D.A. Golombek. Circadian rhythms identified in Caenorhabditis elegans by in vivo long-term monitoring of a bioluminescent reporter. Proc Natl Acad Sci U S A, 113 (2016) 7837-7845.

[29] F. Corellou, C. Schwartz, J.P. Motta, B. Djouani-Tahri el, F. Sanchez, F.Y. Bouget. Clocks in the green lineage: comparative functional analysis of the circadian architecture of the picoeukaryote Ostreococcus. Plant Cell, 21 (2009) 3436-3449.

[30] K.A. Feeney, L.L. Hansen, M. Putker, C. Olivares-Yanez, J. Day, L.J. Eades, . . . G. van Ooijen. Daily magnesium fluxes regulate cellular timekeeping and energy balance. Nature, 532 (2016) 375-379.

[31] L.L. Hansen, G. van Ooijen. Rapid analysis of circadian phenotypes in Arabidopsis protoplasts transfected with a luminescent clock reporter. Journal of visualized experiments : JoVE, (2016) e54586.

[32] S. Hwang, R. Kawazoe, D.L. Herrin. Transcription of tufA and other chloroplast-encoded genes is controlled by a circadian clock in Chlamydomonas. Proc Natl Acad Sci U S A, 93 (1996) 996-1000.

[33] T. Matsuo, K. Okamoto, K. Onai, Y. Niwa, K. Shimogawara, M. Ishiura. A systematic forward genetic analysis identified components of the Chlamydomonas circadian system. Genes Dev, 22 (2008) 918-930.

[34] K. Okamoto, K. Onai, N. Ezaki, T. Ofuchi, M. Ishiura. An automated apparatus for the real-time monitoring of bioluminescence in plants. Anal Biochem, 340 (2005) 187-192.

[35] Y. Xu, T. Mori, C.H. Johnson. Cyanobacterial circadian clockwork: roles of KaiA, KaiB and the kaiBC promoter in regulating KaiC. Embo J, 22 (2003) 2117-2126.

[36] T. Kondo, C.A. Strayer, R.D. Kulkarni, W. Taylor, M. Ishiura, S.S. Golden, C.H. Johnson. Circadian rhythms in prokaryotes: luciferase as a reporter of circadian gene expression in cyanobacteria. Proc Natl Acad Sci U S A, 90 (1993) 5672-5676.

[37] S.A. Bustos, S.S. Golden. Expression of the psbDII gene in Synechococcus sp. strain PCC 7942 requires sequences downstream of the transcription start site. J Bacteriol, 173 (1991) 7525-7533.

[38] H. Shimojo, Y. Harima, R. Kageyama. Visualization of Notch signaling oscillation in cells and tissues. Methods Mol Biol, 1187 (2014) 169-179.

[39] A. Guranowski, J.A. Montgomery, G.L. Cantoni, P.K. Chiang. Adenosine analogues as substrates and inhibitors of S-adenosylhomocysteine hydrolase. Biochemistry, 20 (1981) 110-115.

[40] P.K. Chiang, H.H. Richards, G.L. Cantoni. S-Adenosyl-L-Homocysteine hydrolase-analogs of S-Adenosyl-L-Homocysteine as potential inhibitors. Mol Pharmacol, 13 (1977) 939-947.

[41] C.K. Tseng, V.E. Marquez, R.W. Fuller, B.M. Goldstein, D.R. Haines, H. McPherson, . . . et al. Synthesis of 3-deazaneplanocin A, a powerful inhibitor of S-adenosylhomocysteine hydrolase with potent and selective in vitro and in vivo antiviral activities. J Med Chem, 32 (1989) 1442-1446.

[42] X. Yang, Y. Hu, D.H. Yin, M.A. Turner, M. Wang, R.T. Borchardt, . . . R.L. Schowen. Catalytic strategy of S-adenosyl-L-homocysteine hydrolase: transition-state stabilization and the avoidance of abortive reactions. Biochemistry, 42 (2003) 1900-1909.

[43] K. Brzezinski, Z. Dauter, M. Jaskolski. High-resolution structures of complexes of plant S-adenosyl-L-homocysteine hydrolase (Lupinus luteus). Acta Crystallogr D, 68 (2012) 218-231.

[44] T. Gomi, Y. Takata, T. Date, M. Fujioka, R.R. Aksamit, P.S. Backlund, G.L. Cantoni. Site-directed mutagenesis of rat-liver S-adenosylhomocysteinase-effect of conversion of aspartic acid-244 to glutamic-acid on coenzyme binding. J Biol Chem,

265 (1990) 16102-16107.

[45] D.B. Aultriche, C.S. Yuan, R.T. Borchardt. A single mutation at lysine-426 of human placental S-adenosylhomocysteine hydrolase inactivates the enzyme. J Biol Chem, 269 (1994) 31472-31478.

[46] Y. Takata, T. Yamada, Y.F. Huang, J. Komoto, T. Gomi, H. Ogawa, . . . F. Takusagawa. Catalytic mechanism of S-adenosylhomocysteine hydrolase-Site-directed mutagenesis of Asp-130, Lys-185, Asp-189, and Asn-190. J Biol Chem, 277 (2002) 22670-22676.

[47] T. Yamada, Y. Takata, J. Komoto, T. Gomi, H. Ogawa, M. Fujioka, F. Takusagawa. Catalytic mechanism of S-adenosylhomocysteine hydrolase: roles of His 54, Asp130, Glu155, Lys185, and Aspl89. Int J Biochem Cell Biol, 37 (2005) 2417-2435.

[48] M.W. Sganga, R.R. Aksamit, G.L. Cantoni, C.E. Bauer. Mutational and nucleotide sequence analysis of S-adenosyl-L-homocysteine hydrolase from Rhodobacter capsulatus. Proc Natl Acad Sci U S A, 89 (1992) 6328-6332.

[49] T.A. Bargiello, F.R. Jackson, M.W. Young. Restoration of circadian behavioural rhythms by gene transfer in Drosophila. Nature, 312 (1984) 752-754.

[50] M.W. Young, F.R. Jackson, H.S. Shin, T.A. Bargiello. A biological clock in Drosophila. Cold Spring Harb Symp Quant Biol, 50 (1985) 865-875.

[51] P.E. Hardin, J.C. Hall, M. Rosbash. Feedback of the Drosophila period gene product on circadian cycling of its messenger RNA levels. Nature, 343 (1990) 536-540.

[52] F. Kippert, D.S. Saunders, M.L. Blaxter. Caenorhabditis elegans has a circadian clock. Curr Biol, 12 (2002) 47-49.

[53] T. Saigusa, S. Ishizaki, S. Watabiki, N. Ishii, A. Tanakadate, Y. Tamai, K. Hasegawa. Circadian behavioural rhythm in Caenorhabditis elegans. Curr Biol, 12 (2002) R46-R47.

[54] S. Lee, A.C. Doxey, B.J. McConkey, B.A. Moffatt. Nuclear targeting of methyl-recycling enzymes in Arabidopsis thaliana is mediated by specific protein interactions. Mol Plant, 5 (2012) 231-248.

[55] I. Grbesa, A. Kalo, R. Beluzic, L. Kovacevic, A. Lepur, F. Rokic, . . . O. Vugrek. Mutations in S-adenosylhomocysteine hydrolase (AHCY) affect its nucleocytoplasmic distribution and capability to interact with S-adenosylhomocysteine hydrolase-like 1 protein. Eur J Cell Biol, 96 (2017) 579-590.

[56] T. Matsuo, M. Ishiura. Chlamydomonas reinhardtii as a new model system for studying the molecular basis of the circadian clock. FEBS Lett, 585 (2011) 1495-1502.

[57] G. van Ooijen, M. Hindle, S.F. Martin, M. Barrios-Llerena, F. Sanchez, F.Y. Bouget, . . . A.J. Millar. Functional analysis of Casein Kinase 1 in a minimal circadian system. PloS one, 8 (2013) e70021.

[58] J.S. O'Neill, G. van Ooijen, L.E. Dixon, C. Troein, F. Corellou, F.Y. Bouget, . . . A.J. Millar. Circadian rhythms persist without transcription in a eukaryote. Nature, 469 (2011) 554-558.

[59] G. van Ooijen, L.E. Dixon, C. Troein, A.J. Millar. Proteasome function is required

for biological timing throughout the twenty-four hour cycle. Curr Biol, 21 (2011) 869-875.

[60] P. Sassone-Corsi, The Epigenetic and Metabolic Language of the Circadian Clock. in: P. Sassone-Corsi, Y. Christen (Eds.) A Time for Metabolism and Hormones, Cham (CH), 2016, pp. 1-11.

[61] M. Nakajima, K. Imai, H. Ito, T. Nishiwaki, Y. Murayama, H. Iwasaki, . . . T. Kondo. Reconstitution of circadian oscillation of cyanobacterial KaiC phosphorylation in vitro. Science, 308 (2005) 414-415.

[62] C.H. Johnson, C. Zhao, Y. Xu, T. Mori. Timing the day: what makes bacterial clocks tick? Nat Rev Microbiol, 15 (2017) 232-242.

[63] M. Ishiura, S. Kutsuna, S. Aoki, H. Iwasaki, C.R. Andersson, A. Tanabe, . . . T. Kondo. Expression of a gene cluster kaiABC as a circadian feedback process in cyanobacteria. Science, 281 (1998) 1519-1523.

[64] Y. Liu, N.F. Tsinoremas, C.H. Johnson, N.V. Lebedeva, S.S. Golden, M. Ishiura, T. Kondo. Circadian orchestration of gene expression in cyanobacteria. Genes Dev, 9 (1995) 1469-1478.

[65] X. Qin, M. Byrne, Y. Xu, T. Mori, C.H. Johnson. Coupling of a core post-translational pacemaker to a slave transcription/translation feedback loop in a circadian system. PLoS Biol, 8 (2010) e1000394.

[66] R.D. Walker, J.A. Duerre. S-adenosylhomocysteine metabolism in various species. Can J Biochem Cell B, 53 (1975) 312-319.

[67] P.M. Shih, D.Y. Wu, A. Latifi, S.D. Axen, D.P. Fewer, E. Talla, . . . C.A. Kerfeld. Improving the coverage of the cyanobacterial phylum using diversity-driven genome sequencing. Proc Natl Acad Sci U S A, 110 (2013) 1053-1058.

[68] R.L. Hamil, M.M. Hoehn. A9145, a new adenine-containing antifungal antibiotic. I. Discovery and isolation. J Antibiot (Tokyo), 26 (1973) 463-465.

[69] S.S. Zheng, S. Hausmann, P. Hausmann, Q.S. Liu, A. Ghosh, B. Schwer, . . . S. Shuman. Mutational analysis of Encephalitozoon cuniculi mRNA cap (guanine-N7) methyltransferase, structure of the enzyme bound to sinefungin, and evidence that cap methyltransferase is the target of sinefungin's antifungal activity. J Biol Chem, 281 (2006) 35904-35913.

[70] H. Fujita, K. Syono, Y. Machida, M. Kawaguchi. Morphological effects of sinefungin, an inhibitor of S-adenosylmethionine-dependent methyltransferases, on Anabaena sp. PCC 7120. Microbes Environ, 23 (2008) 346-349.

[71] N. Mashhoon, C. Pruss, M. Carroll, P.H. Johnson, N.O. Reich. Selective inhibitors of bacterial DNA adenine methyltransferases. J Biomol Screen, 11 (2006) 497-510.

[72] R. Kageyama, Y. Niwa, A. Isomura, A. Gonzalez, Y. Harima. Oscillatory gene expression and somitogenesis. Wires Dev Biol, 1 (2012) 629-641.

[73] T. Kobayashi, R. Kageyama. Expression dynamics and functions of Hes factors in development and diseases. Curr Top Dev Biol, 110 (2014) 263-283.

[74] R.A. Rosenberg, M. Abu Haija, P.J. Ryan. Chiral-selective chemistry induced by spin-polarized secondary electrons from a magnetic substrate. Phys Rev Lett, 101

(2008) 178301.

[75] A. Bar-nun, H. Hartman. Synthesis of organic compounds from carbon monoxide and water by UV photolysis. Orig. Life, 9 (1978) 93-101.

[76] P.K. Sarker, J. Takahashi, Y. Obayashi, T. Kaneko, K. Kobayashi. Photo-alteration of hydantoins against UV light and its relevance to prebiotic chemistry. Adv Space Res, 51 (2013) 2235-2240.

[77] M.W. Powner, B. Gerland, J.D. Sutherland. Synthesis of activated pyrimidine ribonucleotides in prebiotically plausible conditions. Nature, 459 (2009) 239-242.

[78] J.S. O'Neill, A.B. Reddy. Circadian clocks in human red blood cells. Nature, 469 (2011) 498-503.

[79] R.S. Edgar, E.W. Green, Y.W. Zhao, G. van Ooijen, M. Olmedo, X.M. Qin, . . . A.B. Reddy. Peroxiredoxins are conserved markers of circadian rhythms. Nature, 489 (2012) 590-590.

[80] Y. Nitanda, T. Matsui, T. Matta, A. Higami, K. Kohno, Y. Nakahata, Y. Bessho. 3 '-UTR-dependent regulation of mRNA turnover is critical for differential distribution patterns of cyclic gene mRNAs. FEBS J, 281 (2014) 146-156.

[81] J. Tan, X.J. Yang, L. Zhuang, X. Jiang, W. Chen, P.L. Lee, . . . Q. Yu. Pharmacologic disruption of polycomb-repressive complex 2-mediated gene repression selectively induces apoptosis in cancer cells. Genes Dev, 21 (2007) 1050-1063.

[82] T.B. Miranda, C.C. Cortez, C.B. Yoo, G. Liang, M. Abe, T.K. Kelly, . . . P.A. Jones. DZNep is a global histone methylation inhibitor that reactivates developmental genes not silenced by DNA methylation. Mol Cancer Ther, 8 (2009) 1579-1588.

[83] M. Zeybel, S. Luli, L. Sabater, T. Hardy, F. Oakley, J. Leslie, . . . D.A. Mann. A proof-of-concept for epigenetic therapy of tissue fibrosis: inhibition of liver fibrosis progression by 3-Deazaneplanocin A. Mol Ther, 25 (2017) 218-231.
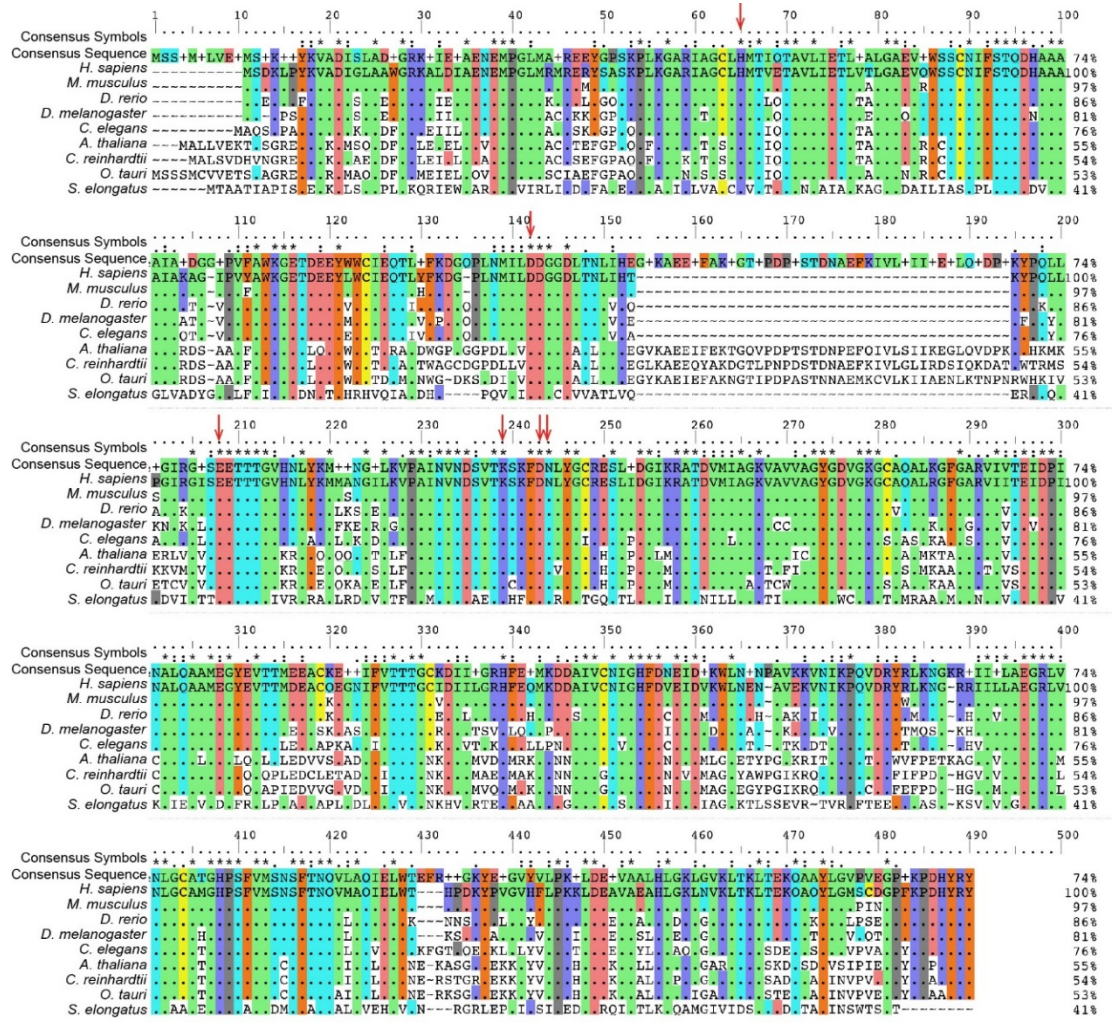
**Figure S1. Sequence alignment of full-length AHCY, related to Fig. 1.**

When amino acids are identical to human, a dot is shown in the alignment. Sequence identities (%), relative to human AHCY, are given on the right. The consensus symbols are shown on top (* = fully conserved residue, : = conservation of strongly similar properties, . = conservation of weakly similar properties). Red arrows indicate the residues that have been reported to be essential for rat AHCY function. The source of sequences is, for human, Genbank: NP_000678.1; mouse, Genbank: NP_057870.3; zebrafish, Genbank: NP_954688.1; fruit fly, Genbank: NP_511164.2; *C. elegans*, Genbank: NP_491955.1; *Arabidopsis*: NP_193130.1; *Chlamydomonas*, Genbank: XP_001693339.1; *Ostreococcus*, Genbank: XP_022839640.1; cyanobacteria, Genbank: WP_011243218.1.
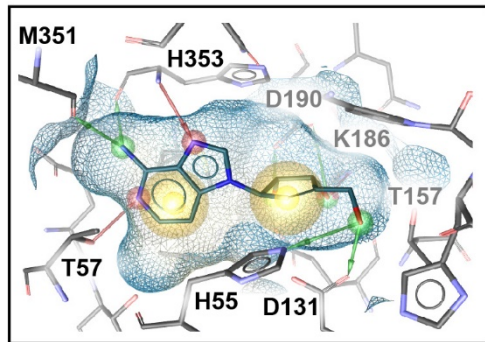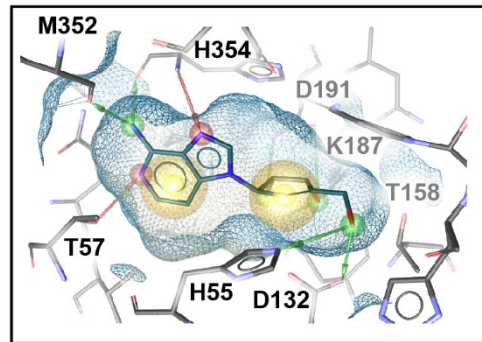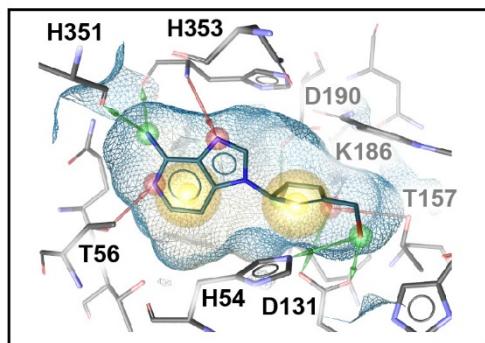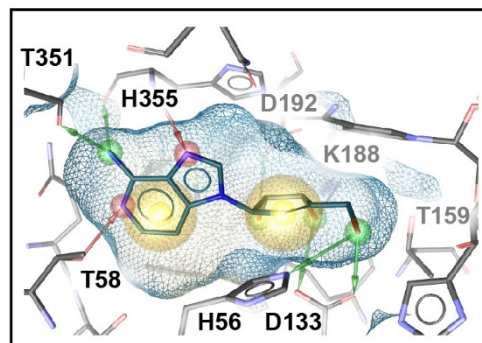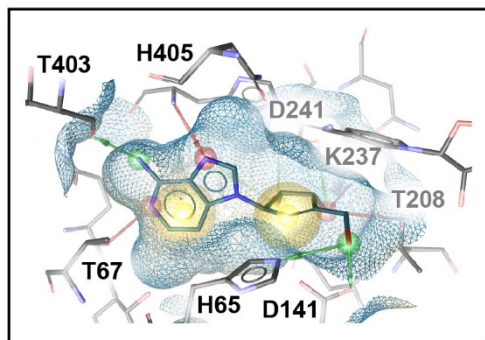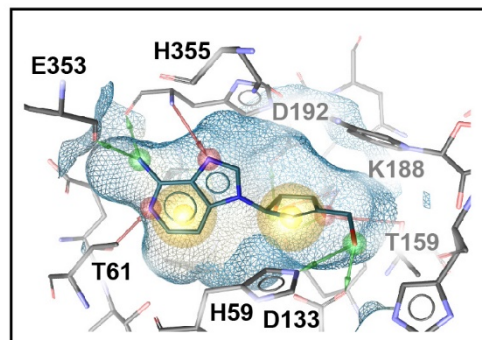
Figure S2. Molecular docking simulations of AHCY with DZnep, related to Fig. 1.

Docking simulations of AHCY with DZnep, for each species as indicated below each picture, based on a published template crystal structure also indicated. The amino acids involved in DZnep binding are indicated together with their position. Note their

conservation. The M351 in mouse (or human, see Fig. 1) is involved in DZnep binding via its backbone, explaining why, although this residue appears at first not conserved (H in fly, T in worm, plants and algae, and E in cyanobacteria), its conserved position in the active site is important. Red and green arrows are hydrogen bonds, yellow spheres are hydrophobic effects. Hydrogen atoms are not shown. The estimated free energies of binding for depicted DZnep docking conformations in kcal/mol were -9.92 for *M. musculus*, -9.50 for D. rerio, -9.29 for *D. melanogaster*, -9.46 for *C. elegans*, -9.50 for *A. thaliana*, -9.26 for *C. reinhardtii*, -9.68 for *O. tauri*, and -9.43 for *S. elongatus*.
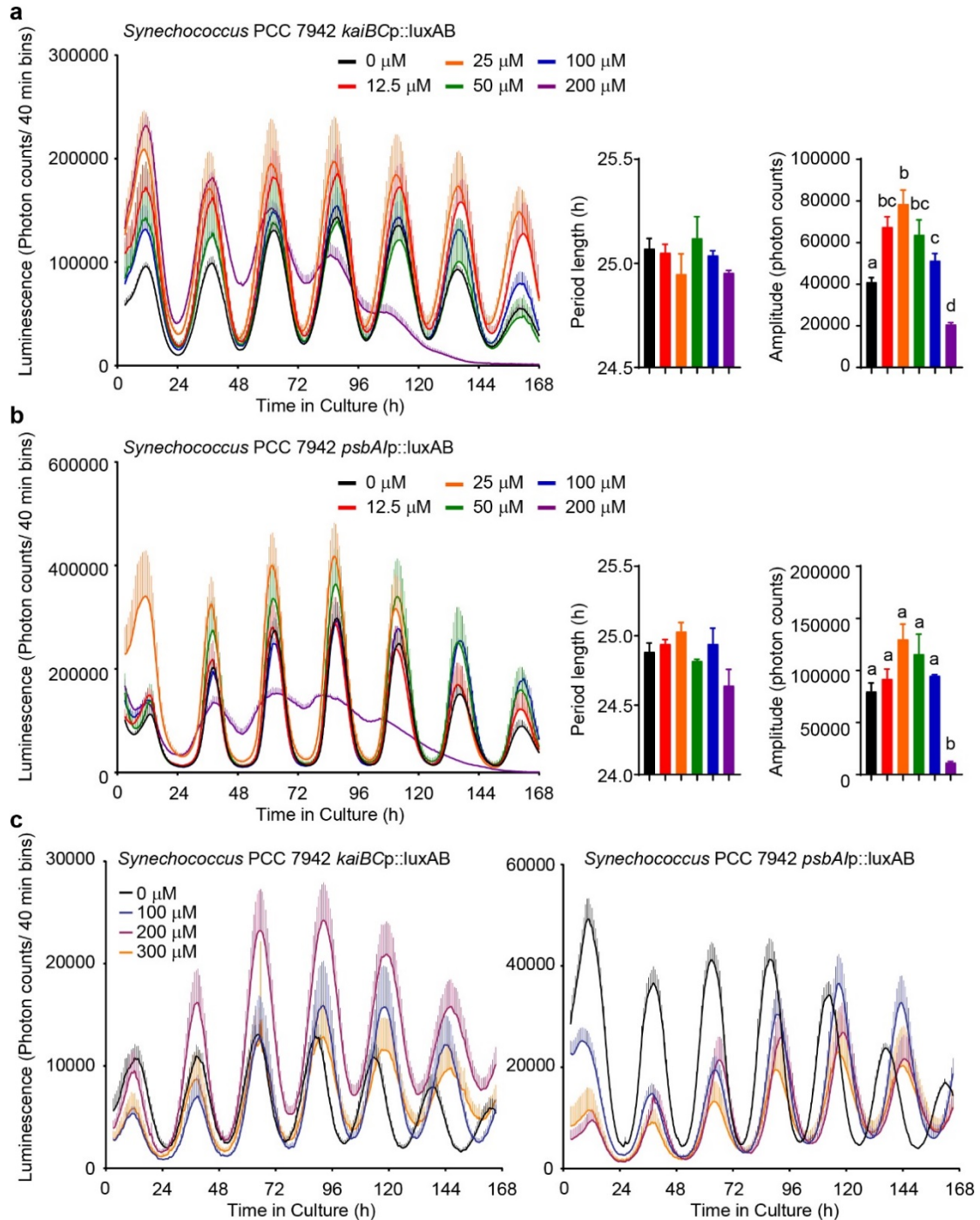
Figure S3. Effects of higher concentrations of DZnep and sinefungin in cyanobacteria, related to Fig. 5. (**a**) Left panel shows mean luminescence +/- SEM of *Synechococcus* PCC 7942 *kaiBCp::luxAB* knock-in strain, n = 3. Middle panel shows mean period +/- SEM of n = 3. Right panel shows mean amplitude +/- SEM of n = 3. (**b**) Same as (a) but using *Synechococcus* PCC 7942 *psbAI*p::luxAB knock-in strain. (**c**) Mean luminescence +/- SEM (n = 3) of *Synechococcus* strains treated with increasing concentrations of sinefungin. All bar graphs analyzed by One-Way ANOVA followed by Bonferroni post-hoc test, *a vs. b vs. c vs. d*, indicating at least $p < 0.05$ significance.
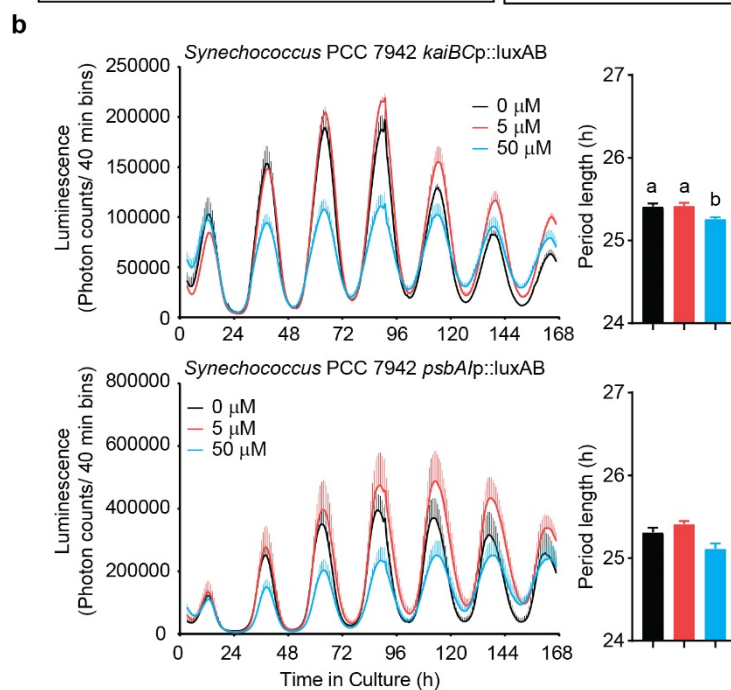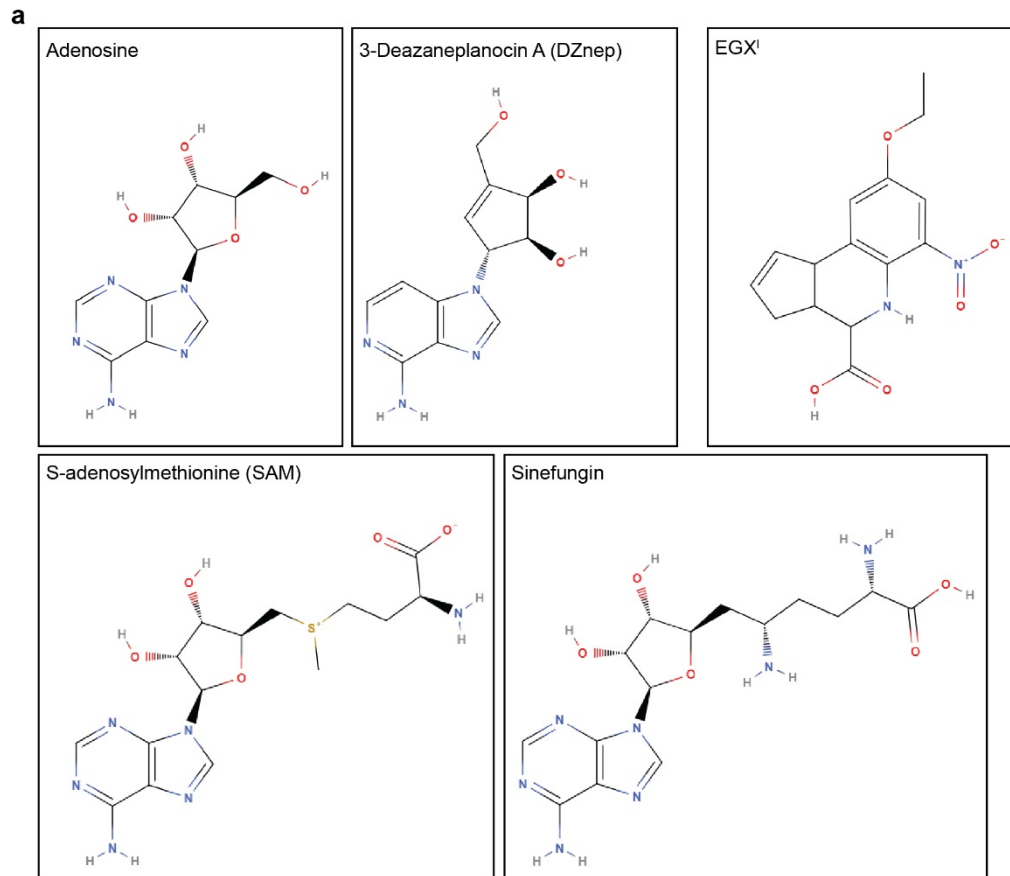
Figure S4. Comparison between the structure and effects of different methylation inhibitors used, related to Fig. 5.

(**a**) Molecular structure of adenosine and its analogue DZnep, which inhibits methylation by binding to the adenosine binding-pocket of AHCY; SAM and its analogue sinefungin, which inhibits methylation by directly binding to

43

methyltransferases; EGX^I, a cyclopentaquinoline carboxylic acid selective bacterial DNA methyltransferase inhibitor. (**b**) Upper left panel shows mean luminescence +/- SEM of *Synechococcus* PCC 7942 *kaiBC*p::luxAB knock-in strain treated with different concentrations of EGX^I, n = 3, with only the upper section of the error bars shown for clarity. Right panel shows mean period +/- SEM, n = 3. Lower panels show similar data but using *Synechococcus* PCC 7942 *psbAI*p::luxAB knock-in strain. All bar graphs analyzed by One-Way ANOVA followed by Bonferroni post-hoc test; *a vs. b*, indicating *p* <0.05 significance.

CHAPTER 2

RNA m6A READER YTHDF2 REGULATES THE CIRCADIAN CLOCK

GRAPHICAL ABSTRACT
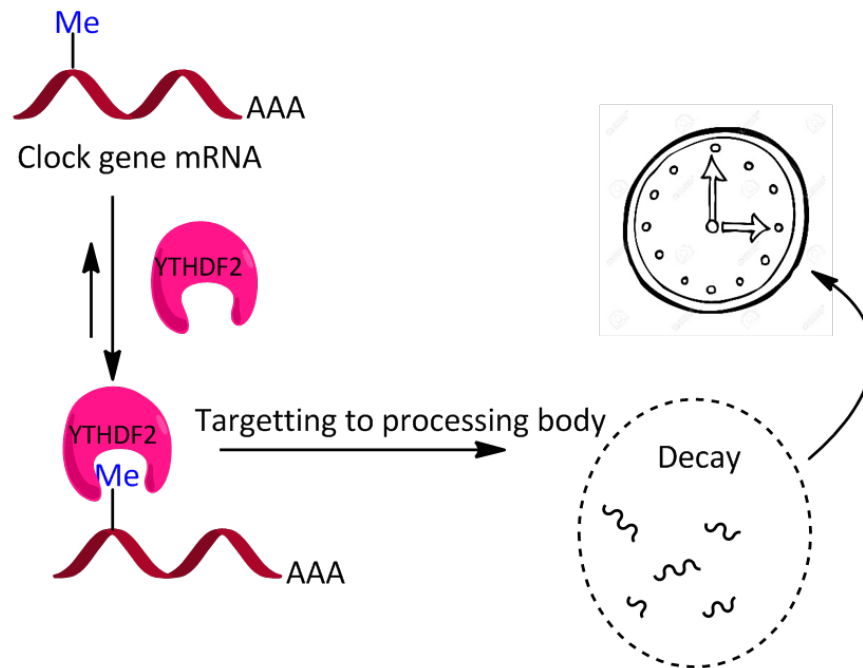
HIGHLIGHTS

Ythdf2 plays a role in circadian process.

Ythdf2 knock-out increases stability of core circadian clock transcripts.

YTHDF2 targets circadian transcripts.

The binding of YTHDF2 to circadian transcripts is sensitive to heat shock stress.

RNA m6A READER YTHDF2 REGULATES THE CIRCADIAN CLOCK

ABSTRACT

Disruption of the methyl cycle has demonstrated to cause the lengthening of circadian period across species, which is at least partially dependent on the N-^{6}-methylation of internal adenosines (m6A) within mRNA rather than DNA methylation. However, how m6A regulates the circadian clock, and in particular the role of m6A "readers", RNA binding proteins that recognize the m6A modification and mediate RNA degradation or translation, is poorly understood. Here, I report that the m6A reader *Ythdf2* plays a critical role in the control of the circadian clock *in vitro*. Specifically, I found that *Ythdf2* knock-down (KD) by siRNA-mediated RNA interference and knock-out (KO) by CRISPR-Cas9 editing led to a lengthened circadian period in mouse cell lines, while exogenous *Ythdf2* overexpression caused a shortened period. The lack of *Ythdf2* expression was associated with an increased stability of mRNAs coding for key components of the transcriptional/translational feedback loop (TTFL) of the circadian clock. Critically, RNA sequencing study revealed that YTHDF2 targets several key clock-related transcripts such as *Per2*, *Cipc* and *Rora*.

Moreover, my results reveal that YTHDF2 localization is dynamic under heat shock conditions, relocating from a mainly perinuclear cytoplasmic distribution to discrete cytoplasmic foci probably corresponding to heat-shock granules and/or P-bodies, which is not consistent with what has been reported by other teams. Together with results showing that the binding of YTHDF2 to clock gene mRNAs decrease after heat shock, this study might help understanding the mechanism of circadian resynchronizing by heat shock.

Overall, this work shows that YTHDF2 at least in part mediates the regulation of

circadian rhythms by m6A, and suggests that YTHDF2 is involved in how the clock respond to heat shock.

INTRODUCTION

The mammalian circadian clock is a cell-autonomous mechanism that is found in all major organ systems and tissues of the body [1]. It is orchestrated by the master clock in the hypothalamic suprachiasmatic nucleus (SCN) [2] that synchronizes the whole body with the environmental light-dark cycles [3].

At the molecular level, the circadian clock involves a transcription-translation auto-regulatory negative feedback loop (TTFL) consisting of the activators CLOCK and its heterodimeric partner BMAL1, and the repressors PER1–3 and CRY1–2. In TTFL network, the CLOCK/BMAL1 heterodimer firstly binds to the regulatory elements called E-box (CAGGTG or CACGTT) in the promoter of *Per* and *Cry* genes to activate their transcription. PER and CRY proteins form PER/CRY multiprotein complexes in the cytoplasm, and then translocate into the nucleus in a tightly regulated manner. In the nucleus, PER/CRY interact with CLOCK/BMAL1 to repress transcription of *Per/Cry* themselves. When this TTFL negative feedback progresses further, mRNA and protein levels of *Per* and *Cry* decrease gradually. Once transcriptional repression is relieved by the turnover of the repressor complex, transcriptional activation by CLOCK–BMAL1 can begin to start a new TTFL cycle [4].

The internal N^6-methyladenosine modification (m6A) in mRNAs is the most prevalent mRNA modification in mammalian cells [5]. m6A mediates a variety of mRNA processing and regulation steps such as splicing [6-8], translation [9, 10] and stability [11, 12], hence plays critical roles in multiple biological processes, including cell development and differentiation [13-16], learning and memory [17], viral infections [18, 19] and cancers [20-24].

Two groups of enzymes are responsible for maintaining the balance of m6A modification: the "writer" and the "eraser" [25]. m6A "writer" is a protein complexes composed of METTL3 [26], METTL14 [27] and Wilms' tumor 1-associated protein (WTAP) [28], which is responsible for adding the methyl mark to adenine in consensus binding motif RR-m6A-CH (R = A or G, H = A or U or C). The "erasers" ALKBH5 [29] and FTO [30] account for removing m6A from mRNA.

In addition, proteins binding to m6A, the "readers", are the functional effectors regulating mRNA processing in an m6A-dependent manner. Three classes of m6A readers have been reported previously. The first class is an m6A-switch mechanism that binds m6A-containing transcripts, including hnRNPC [31], hnRNPG [32] and possibly hnRNPA2B1 [33]. The second class recognizes m6A-containing transcripts using a common RNA-binding domain and flanking regions. For example, IGF2BPs binds m6A-containing RNA with its KH domain selectively [7]. The last class is the YTH domain containing proteins (including YTHDF1, YTHDF2, YTHDF3, YTHDC1 and YTHDC2 in humans) [34] that uses YTH domain to directly bind the m6A [35, 36].

The present study mainly focuses on the m6A reader YTHDF2, which is the firstly identified and best-studied m6A reader among homologues [12, 36-39]. YTHDF2 plays divergent roles that depends on its cellular localization. Under normal conditions, YTHDF2 mainly localizes in the cytoplasm and mediates mRNA decay by selectively recognizing and binding mRNA target that contain a defined G-m6A-CU/A sequence motif via its C-terminal YTH domain [14]. After delocalizing from the actively translating pool, the complex recruits CCR4-NOT mRNA deadenylase complexes and translocates to mRNA decay sites, such as processing body (P-body), through its N-terminal domain to destabilize methylated mRNA [12, 38]. However, under stress conditions such as heat shock, it has been reported that YTHDF2 changes its location from the cytoplasm to nuclei. In the nucleus, the binding of

YTHDF2 to m6A-containing mRNA initiates translation and protects m6A from demethylation by competing against FTO. This function of YTHDF2 appears to be limited to m6A sites located in the 5'-UTR [40]. However, whether FTO is an eraser of m6A or not is still controversial [41]. YTHDF2 also appears to be a major regulator of the proliferation-migration dichotomy (promoting proliferation while suppressing migration), and the ability to invade or adhere [37]. Also, YTHDF2 may serve a role in longevity [42].

In Chapter one, I reported that disruption of the methyl cycle to globally inhibit transmethylations strongly affected the circadian clock in mouse and human cells, which was at least in part explained by m6A inhibition. To further investigate the underlying mechanisms, I sought to determine whether and how YTHDF2 regulates the circadian clock. Here, I show that YTHDF2 targets transcripts coding for clock-related components such as *Per2*, *Cipc* and *Rora* to promote their degradation. Moreover, the association of YTHDF2 with these transcripts was demonstrated to be sensitive to heat shock, with YTHDF2 relocating mainly to heat shock granules/P-bodies.

METHODS AND MATERIALS

Reagents were from Nacalai Tesque unless stated otherwise.

Vectors

Human Flag-tagged *Ythdf2* vector (*hYthdf2*) for Fig. 1d was described previously [12]. Mouse Ythdf2 vector (*mYthdf2*) in Fig. 4b was cloned into the pSELECT-HYGRO-MCS vectors (Invivogen) backbone, with the primers 5'-GACGGATCCGAGAGCCATGTCGGCCAGCAGCCTCTTGGAG-3' and 5'-TATCCATGGCTATTTCCCACGACCTTGACGTTC-3', respectively containing the overhang restriction sites BamHI and NcoI for cloning. Mouse Flag-tagged *Ythdf2* vector for Fig. 5a and Fig. 6b was cloned into *mYthdf2* backbone, with the primers 5'-

GACGGATCCGAGAGCCATGGATTACAAGGACGACGATGACAAGTCGGCCAGCAGCCTCTT

GGAGCAG -3' and 5'- AGTGCTACCTAGGGCTCCTGGTTG -3', respectively containing

the overhang restriction sites BamHI and AvrII for cloning.

Real-time luminescence measurements

Cells were seeded into 35 mm dishes and allow to grow to confluence (typically 3

days). Cells were then shocked by dexamethasone 200 nM for 2 hours, followed by a

medium change including 1 mM luciferine. 35 mm dishes were then transferred to

an 8-dishes luminometer-incubator (Kronos Dio, Atto). Photons were counted in bins

of 2 min (Kronos Dio) seconds (CL24A-LIC) at a frequency of 20 min.

siRNA mediated gene silencing

Gene silencing was performed with Stealth siRNA from Invitrogen. Sequences and

IDs are #45: CCATGATTGATGGACAGTCAGCTTTT and MSS210545; #46:

GGGTGGATGGTAATGGAGTAGGACA and MSS210546. PER2::LUC MEFs plated in

24-well plates at 70,000 cells/ml were transfected the next day with 40-80 pmol

siRNA using 3 µl/well Lipofectamine 3000 (Invitrogen). For RNA analysis by RT-qPCR

shown on Fig. 1b, cells were sampled 24h later. For protein analysis by Western Blot

shown on Fig. 1a and 4b, cells were sampled in 2x SDS sample buffer 36h after

transfection. For PER2::LUC cells and real-time luminescence shown in Fig. 1c, cells

were plated at 70,000 cells/ml in 35 mm dishes, transfected the next day with 320

pmol siRNA and 16 µl Lipofectamine 3000. Sixteen hours later, medium was changed

(antibiotics omitted), and 8 hours later cells were synchronized by a dexamethasone

shock and monitored immediately as described above.

Immunobloting

Cell lysis was conducted in all experiments by using 2x Laemmli buffer supplemented

with Complete protease inhibitor +EDTA (Roche) and Phostop (Roche) followed by

10 min boiling at 95°C. Immunoblots were performed by following standard procedures for migration and blotting with mini-gel (ATTO, Japan). Experimental details for each antibody used were: for YTHDF2, Proteintech 26771-1-AP, 750x or MBL RN123PW, 1000X (IP); for CK1, Proteintech 14388-1-AP, 750x; for METTL3, Proteintech 15073-1-AP, 750x; for β-ACTIN, Sigma A5441, 1000 x; for RPLP0, Proteintech 11290-2-AP.

CRISR-Cas9 genomic editing in MEFs

CRISPR-CAS9 driven mutations were performed using the Addgene vector pSpCas9 (BB)-2A-Puro [43], into which I cloned the sgRNA sequence 5'-GAAGCTGCTTGGTCTACTGG -3'. Transfection of PER2::LUC with the pSpCas9 (BB)-2A-Puro vector was performed using Lipofectamine 3000 following the manufacturer's protocol. After overnight incubation, medium was replaced with medium containing puromycin. After 48 hours, puromycin was removed from the medium and cells were allowed to grow to confluence. Cells were then trypsinized and seeded into 96-well plates at a density of 0.5 cell/well. Clones were allowed to grow sufficiently before being transferred to 24-well plates, plated once more into 24-well plates when confluence was reached. After clonal expansion, the target region of *Ythdf2* was amplified by PCR with primers (5'-GTTGTGAATGATGATGTGGAAGG-3' and 5'-GTAGACTGTCCCTGAGAACT-3') and subjected to BpmI digestion and then Sanger sequencing. Finally, two Ythdf2 knock-out monoclonal cell lines were obtained.

Cell preparation and YTHDF2-RIP

Ribonucleoprotein immuno-purification (RIP) assay was conducted using the Magna RIP RNA-Binding Protein Immunoprecipitation Kit (Millipore, Bedford, MA, USA) according to the manufacturer's protocol. Briefly, for exogenous *Ythdf2*, PER2::LUC cells were harvested 36h after transfection with *Ythdf2* vector then lysed in RIP lysis

buffer. Subsequently, 100μl cell extract was incubated with RIP buffer containing magnetic beads conjugated with 5μg mouse anti-Flag antibody or 5μg normal mouse IgG as negative control. For endogenous YTHDF2 RIP, PER2::LUC cells were harvested then lysed in RIP lysis buffer. After that, 100ul cell extract was incubated with RIP buffer containing magnetic beads conjugated with rabbit anti-YTHDF2 antibody or normal rabbit IgG as negative control. Proteinase K was used to digest the protein and the immunoprecipitated RNA was purified. The isolated RNA was used for RT-qPCR or cDNA library construction and RNA sequencing.

YTHDF2-RIP with RNA-seq

For wild-type and *Ythfd2* knock-out cells, raw reads from input and YTHDF2-RIP Fastq files were first trimmed and quality-filtered (Trimmomatic) then aligned to the reference genome mm10 with RNAstar [44]. Gene count tables were obtained by StringTie [45, 46]. These analyses were performed on the Galaxy server. Raw sequencing reads and count table from Stringtie are available at https://data.mendeley.com/datasets/4b9byd5pm6/draft?a=8a4114ca-9393-4e31-a364-9f1204b1c119 (Mendeley Data).

Immunocytochemistry

Immunocytochemistry was performed on glass chamber slides (Labtek). The day after plating, cells were incubated in different temperature incubator for the indicated time, chambers were detached from the slides and cells were briefly rinsed once with PBS before fixation with 4% PFA in PBS for 10 min at RT. After three 5 min washes in PBS at RT, cells re permeabilised in 0.2% TX-100 in PBS for 20 min at 4°C. After three 5 min washes in PBS at RT, cells were blocked for 2 hours in PBS 0.2% Tween-20, 5% BSA, 5% FBS at RT. Cells were then incubated overnight in PBS 0.2% Tween-20, 1% BSA, 1% FBS, containing the appropriate primary antibodies (YTHDF2, Proteintech 26771-1-AP, 600x) at 4°C. After three 5 min washes on PBS 0.2%

Tween-20 at RT, cells were further incubated in PBS 0.2% Tween-20, 1% BSA, 1% FBS, containing the appropriate secondary antibodies (anti-Rabbit Alexa 594, Invitrogen 461 A-21207, 1 ug/ml) for 2h at RT in the dark. Cells were then washed three times 10 min in PBS 0.2% Tween-20, two times 10 min in PBS, then rinsed briefly in deionized water before mounting with Prolong antifade Gold reagent with DAPI (Invitrogen) for 24h. Cells were imaged with a Zeiss microscope, and for each wavelength, frames were acquired with the same exposure time and identical brightness and contrast parameters.

Heat shock and its resetting calculation

Mouse PER2::LUC were cultured to confluence in DMEM/F12 with 10% fetal bovine serum at 37ºC, treated with 200nM Dexamethasone for 2 hours before the start of measurements. For immunohistochemistry and RIP, cells were heat shocked (42ºC, 1 hour) then harvested directly or after recovery at 37°C for 1 or 2 hours. For real-time luminometry, the medium was changed to DMEM/F12 with 10% fetal bovine serum and 1mM Luciferin. Cells were then transferred to the luminometer-incubator (Kronos Dio, Atto) where bioluminescence was recorded at intervals of 20 min at 37°C, 5% CO2. Heat shock pulse (42°C, 1 hour) was applied during the increasing phase of PER2::LUC luminescence, more than 36 hours post dexamethasone treatment to avoid any potential effects of dexamethasone. Circadian period for each treatment group was normalized to 24 circadian hours in order to allow comparison between phase-shifts occurring in WT and *Ythdf2* KO. The times of PER2::LUC troughs before (x) and after (y) the heat shock were recorded, as well as the subsequent trough time in constant conditions to estimate endogenous period length (t). Phase shifts were then calculated and normalized by the equation:

$$\frac{(y - x) \times T}{t} - T$$

where T is the normalized endogenous period length (24 h).

RNA extraction and RT-qPCR

Total RNA was extracted with RNeasy kit (Qiagen) and transcribed to cDNA with SuperScript VILO cDNA Synthesis kit (Invitrogen). RT-qPCR was performed following standard protocol with SYBR Green PCR Master Mix (Invitrogen) on a StepOne Real-Time PCR Systems (Applied Biosystems) (Fig 5c, 6d, 6e) or on a BioMark HD System (Fluidigm) with a 48_48 Fluidigm BioMark Dynamic Array chip (Fluidigm) (Fig 3a). Primers were shown as below.

Primer sequences for quantitative real-time PCR

For *Bmal1* 5'- AGGCGTCGGGACAAAATGAACA -3' and 5'-TGGGTTGGTGGCACCTCTCA -3'

For *Bhlhe40* 5'- ACCTCCTACCTGCCTGCCCA -3' and 5'- TCCGTTTTATTCCCCGCCTG -3'

For *Clock* 5'- GGGTCTATGCTTCCTGGTAA -3' and 5'- TCCTGTCGAATCTCACTAGC -3'

For *Crebbp* 5'- CCAGTTTCCATCATCCAGTG -3' and 5'- CAGCATGTTCAGAGGGTTAG -3'

For *Cry1* 5'- CTCGTCTGTTTGTGATTCGGG -3' and 5'- AGCTGCATCTCGTTCCTTCC -3'

For *Cry2* 5'- TGACGCCATCATGACCCAAC-3' and 5'- AGGAGCAGCTCGTCAAATAC-3'

For *Ck1δ1* 5'- CGCATGTCCACCTCACAGATTCC -3' and 5'- GGTAACAGAGTAGATCAGCC-3'

For *Ck1δ2* 5'- CTGCTCGTCTCCATCGGAAG -3' and 5'- ACAGAGTAGATCAGCCATGC-3'

For *Ck1ε* 5'- GAGACATCTACCTGGGTGCCA -3' and 5'- ACCACTTGATGGACGGGATC-3'

For *Nfil3* 5'- GGAGCAGAACCACGATAACC -3' and 5'- CCCCAGTCTTCTTTCAGGTC-3'

For *Per1* 5'- GCAGGTTCAGGTCTCAAGGACT -3' and 5'- GTTAGGCGGAATGGCTGGTA-3'

For *Per3* 5'- CAGAGCCTTGCTGTCTAACA -3' and 5'-

GAAACACACATCCTGGAGTG-3'

For *36b4* 5'- CTCACTGAGATTCGGGATATG -3' and 5'-

CTCCCACCTTGTCTCCAGTC-3'

For *Ythdf2* 5'-CCAATAATAGCCCACCAGTG -3' and5'-GTCCTACTCCATTACCATCCAC-3'

TaqMan probe and primer sets were as follows;

For *Per2*, probe, FAM-AGGCACCTCCAACATGCAACGAGCC-

TAMRA, forward primer (fw): 5'-GCACATCTGGCACATCTCGG-3', reverse primer (rv):

5'-TGGCATCACTGTTCTGAGTGTC-3';

For *Per1*, probe, FAM-AGCCCCTGGCTGCCATGG-TAMRA, fw:
5'-CAGGCTTCGTGGACTTGAGC-3', rv: 5'-AGTGGTGTCGGCGACCAG-3';

For *Per3*, probe, FAM-TTCTGCTCATCACCACCCTGCGGTTCC-TAMRA, fw:
5'-ACAGCTCTACATCGAGTCCATG-3', rv: 5'-CAGTGTCTGAGAGGA AGAAAAGTC-3';

For *Cry1*, probe, FAM-TGATCCACAGGTCACCACGAGTCAGGAA-TAMRA, fw:
5'-TAGCCAGACACGCGGTTG-3', rv:
5'-AGCAGTAACTCTTCAAAGACCTTC A-3';

For *Cry2*, probe, FAM-AGGTCTCTCATAGTTGGCAACCCAGGC-TAMRA, fw:
5'-TGGACAAGCACTTGGAACGG-3', rv: 5'-GGCCAGTAAGGAATT GGCATTC-3';

For *Clock*, probe, FAM-ACCCAGAATCTTGGCTTTTGTCAGCAGC-TAMRA, fw:
5'-TGGCATTGAAGAGTCTCTTCCTG-3', rv: 5'-GAGACTCACTGTGTT GATACGATT G-3';

For *Bmal1*, probe, FAM-CGCCAAAATAGCTGTCGCCCTCTGATCT-TAMRA, fw:
5'-GTACGTTTCTCGACACGCAATAG-3',

rv: 5'-GTACCTAGAAGTTCCTGTGGTAGA-3';

RESULTS

<u>*Ythdf2* knock-down extends circadian period while *Ythdf2* overexpression accelerates the period in PER2::LUC cells</u>

56

To test the potential effect of Ythdf2 on the circadian clock, *Ythdf2* KD was firstly tested in mouse embryonic fibroblasts (MEFs) carrying a heterozygote fusion between the coding sequence of the core clock protein PER2 and luciferase (PER2::LUC). RT-qPCR and western blotting were performed to validate the successful mRNA and protein knock-down (Fig 1a, b), and the *Ythdf2* KD had no observable effect on cell viability. The results showed that Ythdf2 KD leads to the lengthening of the circadian period with two different siRNA, #45 and #46, targeting different regions in *Ythdf2* (Fig 1c).

To further confirm the regulatory role of YTHDF2 on the circadian clock, an expression vector for human YTHDF2 was transiently transfected into PER2::LUC MEFs. As expected, overexpression of YTHDF2 accelerates the circadian period (Fig 1d, e). These results, both KD and overexpression, provide direct evidence that YTHDF2 regulates the circadian clock.

Ythdf2 knock-out lengthens the circadian period in PER2::LUC

To further investigate the role of *Ythdf2* in the circadian clock, I knocked-out *Ythdf2* in PER2::LUC cells using CRISPSR-Cas9. Two clonal cell lines (KO#1 and KO#2) were generated by using single-guide RNA (sgRNA) targeting the exon 1 of the *Ythdf2* gene to introduce indels in order to abolish *Ythdf2* expression, which was confirmed by western blotting (Fig 2a, see also Fig. 4a and 4b). Consistent with the KD results, the two *Ythdf2* KO cell lines had significantly lengthened circadian periods compared to wild-type (WT) controls (Fig 2b). Since the networks of the circadian clock and cell proliferation are often mutually linked, I also investigated the effect of *Ythdf2* KO on cell proliferation. The results showed that *Ythdf2* KO cells had a dramatically slower proliferation rate than wild-type controls (Fig. 2c), which is consistent with a previous report showing that YTHDF2 promotes cell proliferation in tumor cells [37]. Collectively, these results demonstrate that the circadian clock is regulated by m6A

methylation at least partly mediated by the reader YTHDF2.

Ythdf2 knock-out increases the stability of key circadian transcripts

As a selective mRNA m6A binding protein, YTHDF2 supervises mRNA degradation by dragging the bound m6A-containing transcript away from the translation machinery to RNA decay sites, such as P-body, and ultimately affects mRNA half-life and translation [12].

By using high-throughput RT-qPCR, I confirmed that *Ythdf2* KO significantly increased the stability of circadian clock transcripts. For example, the members of the clock positive loop, mRNAs of *Arntl1*, *Arntl2* and *Clock*, were clearly more stable in *Ythdf2* KO cells compared to WT. The members of the clock negative loop, the three *Per1–3* mRNAs and the two *Cry* mRNAs (*Cry1–2*) were also more stable in *Ythdf2* KO cells compared to WT (Fig 3a). So were the other circadian clock-controlled genes such as *Bhlhe40*, *Bhlhe41*, *Rora*, *Dbp* and *Nfil3*.

The influence of *Ythdf2* KO on clock mRNA levels was also investigated (Fig 3b). The results showed that most of clock mRNAs, including *Per1*, *Per2*, *Per3*, *Rora*, *Nr1d1*, *Dbp* and *Ck1δ1*, were significantly increased, which is consistent with their higher stability shown in Fig. 3a. Although the stability of *Bmal1*, *2* and *Clock* was increased, their transcripts did not show significant changes steady-state levels.

Ythdf2 knock-out decreases translation of target mRNA

It has been reported that, although *Ythdf2* KD increases the stability and steady-state levels of many target transcripts, it is also associated with reduced translation efficiency due to the accumulation of mRNA pool in a non-translating state [12]. In agreement with these studies, I also found that *Ythdf2* KO lowered the protein expression levels of METTL3, CK1δ and RPLP0. In contrast, the β-ACTIN level was not changed, consistent with the *β-actin* mRNA not being a target of YTHDF2 due to its

lack of or low m6A-methylation [47, 48] (Fig 4a). To overturn the effect of *Ythdf2* KO on translation, *mYthdf2* was exogenously re-expressed in PER2::LUC in *Ythdf2* KO MEFs (Fig 4b). As expected, the re-expression led to an increase in the METTL3, CK1δ and RPLP0 levels, but not β-ACTIN level.

I thus hypothesize that YTHDF2 not only initiates degradation but is also capable to recruit other proteins in some cases, such as YTHDF1, that decrease the translation of its targets [10]. It is also possible that YTHDF2 and YTHDF1 compete with the same methylated binding sites, resulting in antagonistic or more complex regulation [49]. Another explanation is that YTHDF2 itself is capable of inhibiting translation of some target transcripts, which depends on the location of m6A site. It is worthwhile to mention that all members of the YTH domain containing family have the ability to regulate translation and RNA degradation of viral RNA transcripts [50, 51].

YTHDF2 binds mRNA of circadian clock genes in RIP-seq assay

To identify circadian clock-related mRNA targeted by YTHDF2, I next performed immunopurification of ribonucleoprotein complex (RNP) combining RT-qPCR (RIP-qPCR) in PER2::LUC cells that were transfected with a FLAG-tagged YTHDF2 expression vector. The results from RIP-qPCR assay showed that clock-related transcripts, including *Bmal1*, *Clock*, *Per*, *Cry*, *Ck1δ* and *Ck1ε,* were markedly enriched in FLAG-YTHDF2 overexpressing cells compared to control PER2::LUC cells (Fig 5a, b, c). To further identify targets of endogenous YTHDF2 in a non-biased manner, RIP combined with RNA sequencing (RIP-Seq) was performed on WT PER2::LUC cells and two *Ythdf2* KO cell lines. I first confirmed that YTHDF2 antibody was appropriate for RIP-Seq (Fig 5d). Among 12,695 genes with an expression over the ratio of 10 (FPKM) in PER2::LUC cells, 731 transcripts were at least 2 folds highly enriched in the IP fraction of WT cells compared to that of the average of *Ythdf2* KO cells (Fig 5e). Among clock-related transcripts were *Cipc* (6.9-fold), *Rora* (5.9-fold) and *Per2*

(2.0-fold). Other notable transcripts that have high m6A levels reported previously were *Creb1* (6.9-fold), the key methyl cycle enzyme *Mat2a* (3.9-fold) and the mRNA cap-binding protein *Dcp1b* (3.7-fold) that were enriched in the WT IP fraction (Fig 5f). Altogether these data support my hypothesis that at least some clock-related transcripts are bound by the m6A reader YTHDF2.

Compared with my RNA-seq results obtained from RNA immunoprecipitation using the anti-YTHDF2 antibody on endogenous YTHDF2, overexpression of a FLAG-tagged YTHDF2 led to an increase in the detected enrichment of co-immunoprecipitated clock-related transcripts. It is likely that overexpression of YTHDF2 disrupted the delicate balance between m6A readers and displaced the other YTH homologues from their respective target transcripts.

YTHDF2 effectively adjusts its cellular localization under heat shock

Besides being an m6A reader, YTHDF2 has been reported to bind m6A "writer" complexes including METTL3, METTL14 and WTAP and change its co-localization after the recovery from heat shock [52]. Furthermore, it has been shown in MEFs that after two hours recovery from heat shock, YTHDF2 translocates to the nucleus where it protects m6A sites in the 5'-UTR from demethylation by the m6A 'eraser' FTO, leading to the induction of cap-independent translation [40]. Since heat shock can re-synchronize the circadian clock [53], I sought to investigate whether heat shock could also induce YTHDF2 nuclear translocation in PER2::LUC MEFs and in particular, the mechanism of circadian clock synchronization by heat shock. Against my expectations, after one hour heat shock at 42°C, YTHDF2 mainly relocated to cytoplasmic heat shock/stress granules (and/or P-body) and to discrete nuclear stress granules-like structures [54] (Fig. 6a), but not to the exclusive diffuse nuclear distribution as previously reported [40]. The YTHDF2-positive heat shock granules progressively disappeared during the recovery condition at 37°C (Fig 6a).

Next, I sought to determine whether the binding of YTHDF2 to its target mRNAs was

altered during heat shock. By immunopurification of YTHDF2 complexes followed by qPCR, the results revealed that heat shock dramatically reduced the enrichment of YTHDF2-associated transcripts, including *Bmal1*, *Clock*, *Per*, *Cry*, *Ck1δ*, *Ck1ε* and *Ythdf2* itself. After two hours recovery at 37°C, the enrichment of these mRNA in the YTHDF2-immunoprecipitated RNP complex was partially recovered (Fig 6b, c). Heat shock did not affect the expression level of most YTHDF2 sensitive transcripts (Fig 6d).

Lastly, to determine whether YTHDF2 is involved in the resetting effect of heat shock on the circadian clock, heat shock was performed on wild-type and *Ythdf2* KO PER2::LUC cell lines. A one hour heat shock at 42°C during the increasing phase of PER2::LUC luminescence lead to a phase advance of over 1 hour in wild-type cells, while the two *Ythdf2* KO cell lines seemed to present a blunted response, but because of limited replicates number significance was not reached (Fig. 6e). Nonetheless, these data support my hypothesis that YTHDF2 regulates the circadian clock.

DISCUSSION

In 2013, our lab reported that m6A was a circadian pacemaker in mouse and human cells [55]. In 2018, our lab reported that the 3'-UTR region of *Ck1δ*, coding for the casein kinase 1 delta, a key regulator of circadian rhythms, was heavily methylated, led to the characterization of two functionally antagonistic isoforms of CK1δ, both regulated by m6A [8, 56]. However, how m6A regulates the circadian clock, and in particular the role of m6A "reader", is poorly understood.

This research investigated the role of YTHDF2 in the m6A-dependent regulation of the circadian clock and sought to give direct evidence that YTHDF2 targets circadian clock transcripts. The data clearly demonstrated that *Ythdf2* depletion extends the circadian period while YTHDF2 overexpression accelerates the period. Consistent

with the observations that the stability of many clock-related transcripts increases in m6A-deficient cells [55], I here show that the m6A reader YTHDF2 directly or indirectly targets clock-related transcripts for degradation.

For the heat-shock experiments, I used the same antibody as Zhou and coworkers [40], and my experiments were also performed in MEFs. Since the YTHDF2 distribution under normal conditions I reported was virtually identical to that shown by these authors, these discrepancies are not easy to explain. It is noteworthy to mention that Donal O'Carroll lab at the University of Edinburgh also failed to reproduce the data reported by Zhou *at al*. (personal communication). Indeed, a very recent report showed that, after heat shock, YTHDF2 does translocate to stress granules, not to the nucleus [57].

Stress granules are very dynamic structures that exchange components with the cytoplasm. They contain untranslating messenger ribonucleoproteins (mRNPs) that can be formed at any stage of the lifetime of the transcript, i.e., directly after export to the cytoplasm, after association with the translation initiation factors and even after binding to ribosome [58]. Stress granules can interact with P-bodies and undergo autophagy. I propose that under heat shock stress at 42°C, YTHDF2 mediates entry of unstranslating mRNPs to stress granules, where its target mRNAs are degraded. Some YTHDF2 may move to the nucleus to promote cap-independent translation of mRNA involved in heat shock response, maybe explaining why YTHDF2, promoted by its increase after heat shock. This hypothesis is consistent with the ICC result in my experiment. Moreover, *Ythdf2* KO appeared to blunt the resetting of the clock after heat shock, but more experiments, notably with a longer heat shock, will be needed to confirm this.

Further investigations using *Ythdf2* KO mice should confirm whether YTHDF2

regulates the circadian clock *in vivo*. However, as a key regulator of folliculogenesis [14], *Ythdf2* deficiency leads to female infertility and is embryonic semi-lethal, causing eye malfunctions in surviving mice [48], which may complicate investigations in the circadian rhythms of *Ythdf2* knock-out mice. Tissue-specific knock-out, for example, targeting the suprachiasmatic nucleus, or an inducible knock-out design, will be used for the future investigations.
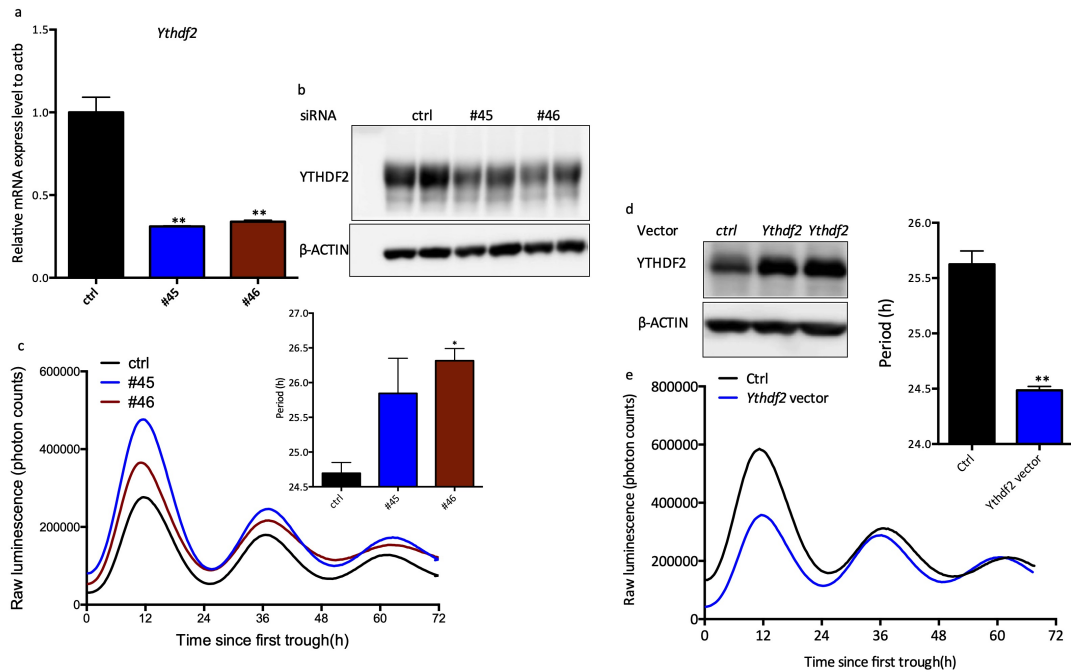
Figure 1. Ythdf2 knock down elongates circadian period while overexpression Ythdf2 accelerates the period in PER2::LUC

(**a**) Quantification of the *Ythdf2* mRNA level relative to *36b4* post *Ythdf2* KD in the PER2::LUC, ΔCT data analyzed by Student *t*-test, shown as mean ± SEM, n=3, ***p <0.01. (**b**) Validation of *Ythdf2* KD by immunoblotting, showing a decrease in YTHDF2, with β-ACTIN used as a loading control. (**c**) *Ythdf2* silencing causes period lengthening. The period was estimated by BioDare2. (**d**) Overexpression of YTHDF2 was confirmed by immunoblot, with β-ACTIN used as a loading control. (**e**) YTHDF2 overexpression leads to period shortening. The period was estimated by BioDare2. Insert shows the period analyzed by Student *t*-test, data shown as mean ± SEM, n=3, ***p <0.01.
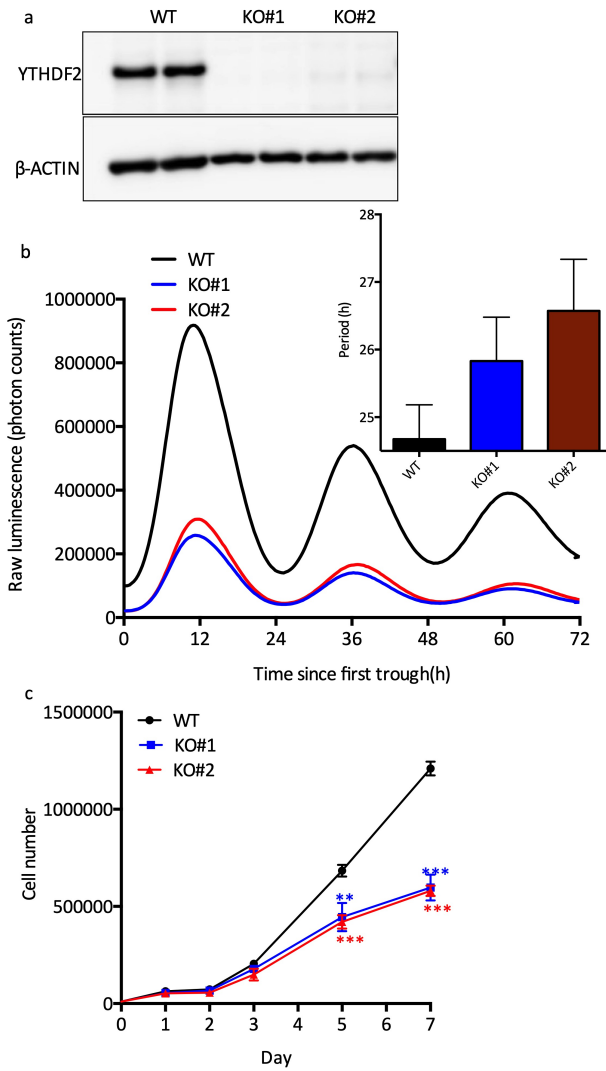
Figure 2. Ythdf2 knock out elongates circadian period in PER::LUC

(**a**) Validation of two *Ythdf2* KO clonal PER2::LUC cell lines, termed as KO#1 and KO#2 and β -ACTIN was used as a loading control. (**b**) *Ythdf2* deletion causes period lengthening. The period was estimated by BioDare2. (**c**) *Ythdf2* deletion leads to low proliferation potential. The cell number analyzed by student *t*-test, and shown as mean ± SD, n=3, **p <0.01, ***p <0.001.
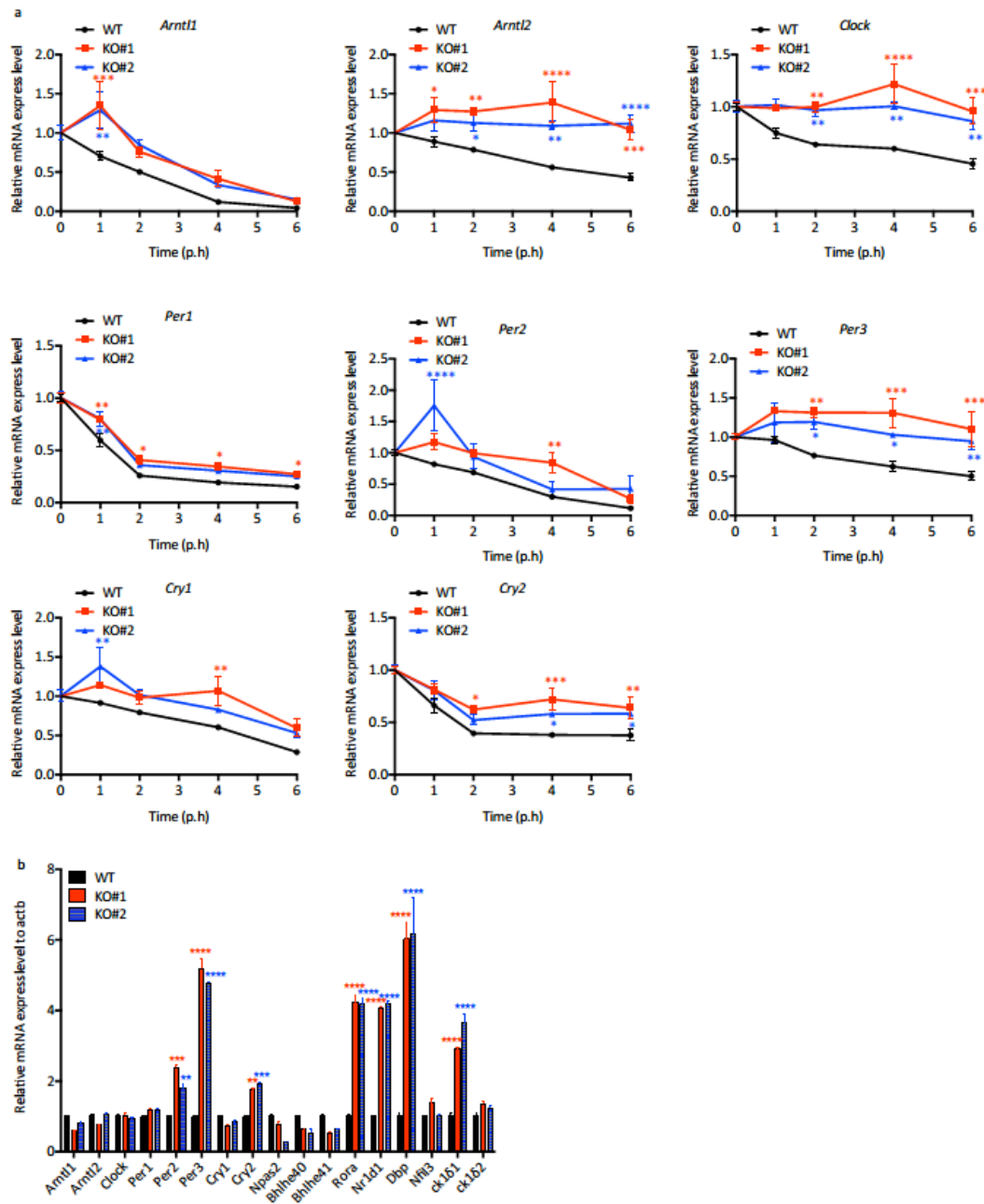
Figure 3. Ythdf2 knock out increases the RNA stability of main circadian genes

(**a**) The stability of many clock-related transcripts increases in *Ythdf2* KO cells compared to WT. Quantification of the mRNA levels at 0, 1, 2, 4, 6h after Actinomycin D from n=3 experiments and ΔCT analyzed by Two-Way ANOVA, data shown as mean ± SEM, *p <0.05, **p <0.01, ***p <0.001, ****p <0.0001. (**b**) *Ythdf2* KO leads to increased steady-state levels of *Per2*, *Per3*, *Cry2*, *Rora*, *Nr1d1*, *Dbp* and *Ck1δ* mRNA levels relative to *Actb*. ΔCT data analyzed by student *t*-test, and shown as mean ± SEM, n=3, **p <0.01, ***p <0.001, ****p <0.001.
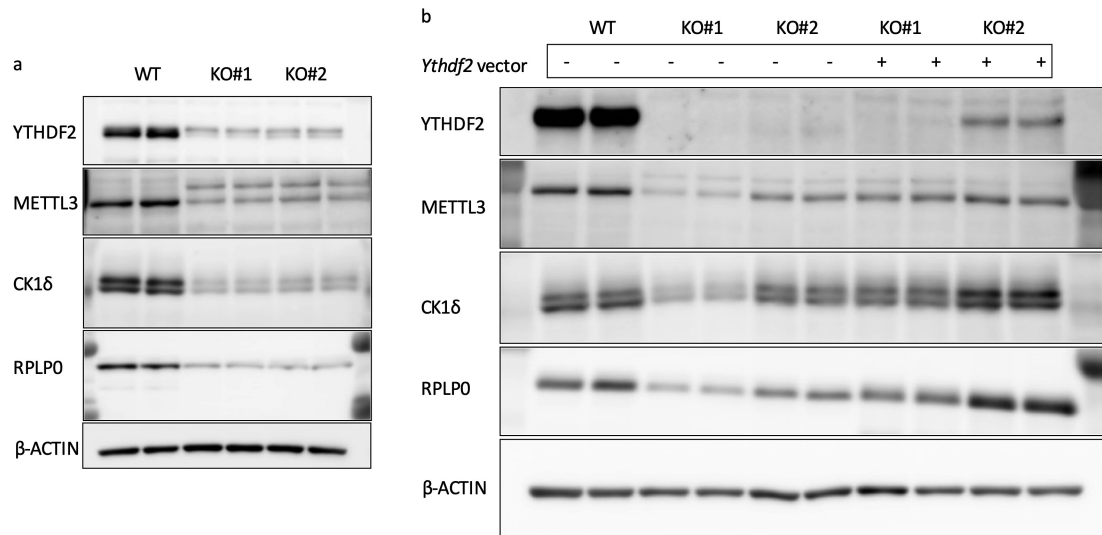
Figure 4. Ythdf2 KO decreases translation

(**a**) *Ythdf2* deletion in PER2::LUC decreases levels of METTL3, CK1δ, RPLP0 but not β-ACTIN which was used as a loading control. (**b**) Exogenous expression of *Ythdf2* in *Ythdf2* KO cells rescued METTL3, CK1δ, RPLP0 expression but not β-ACTIN which also was used as a loading control.
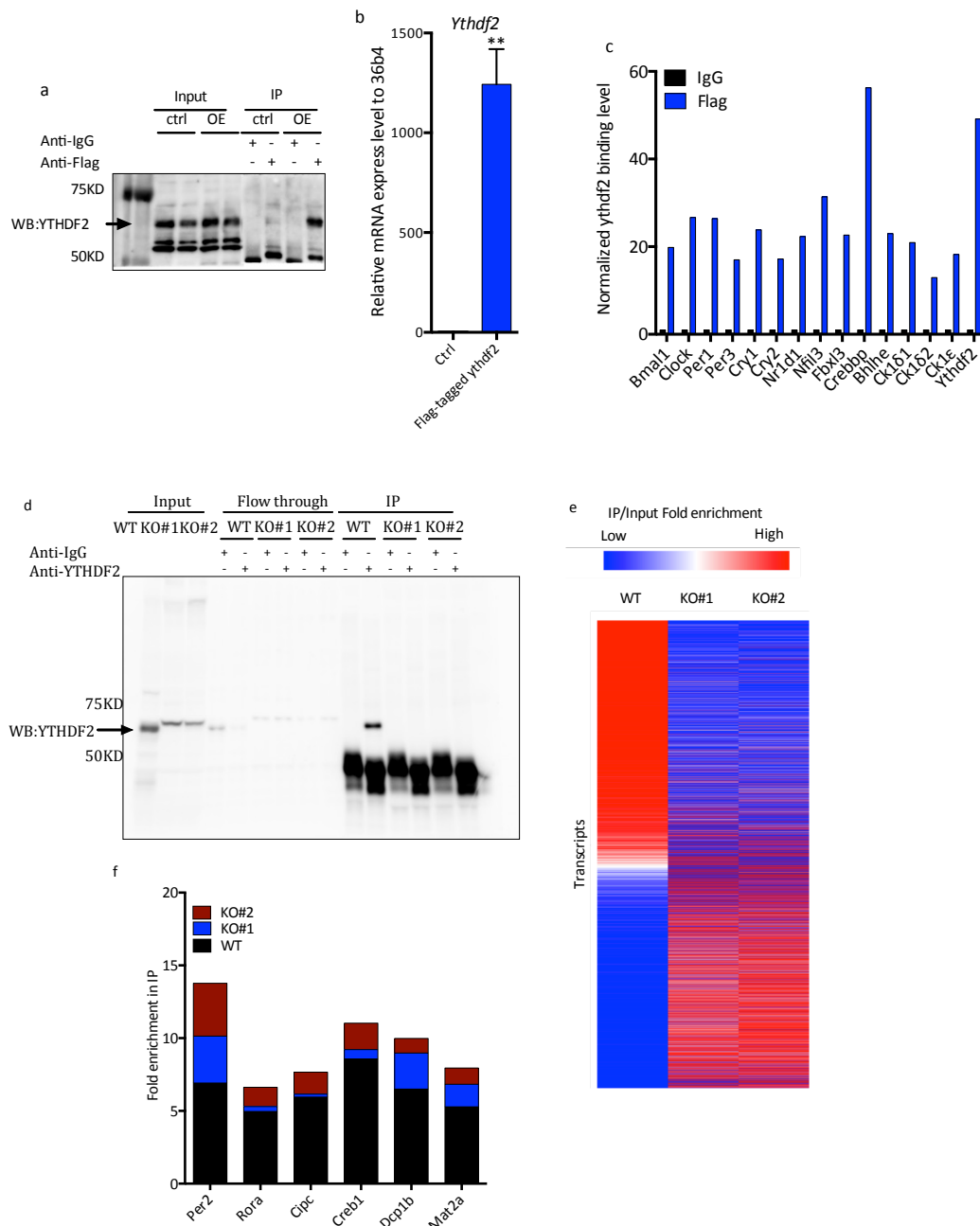
Figure 5. YTHDF2 binds to specific circadian clock target

(**a**) Immunoprecipitation of a transfected flag-tagged YTHDF2, using anti-FLAG antibody. Mouse IgG was used as a negative control for immunoprecipitation. OE indicates FLAG-YTHDF2 transfected cells, ctrl transfection with the empty vector backbone. (**b**) Overexpression was confirmed by qPCR after flagged-tagged *Ythdf2* vector transfection. ΔCT data was relative to *Actb*, analyzed by student *t*-test, data shown as mean ± SEM, n=3, **p <0.01. (**c**) Binding of circadian clock-related transcripts to FLAG-YTHDF2, identified by FLAG-YTHDF2-RNA ImmunoPrecipitation (RIP) combided with RT-qPCR. (**d**) Validation of anti-YTHDF2 antibody for RIP with

cell lysates from WT and *Ythdf2* KO PER2::LUC lysates. Rabbit IgG was used as negative control for IP. (**e**) Heatmap of IP/INPUT fold-enrichment values of 12,695 transcripts in WT and *Ythdf2* KO cells, identified by YTHDF2 RIP followed by RNA-seq. From top to bottom transcripts are sorted according to their decreasing relative enrichment in WT cells. (**f**) Fold-enrichment of selected transcripts from e, with associated expression levels in the INPUT fraction.
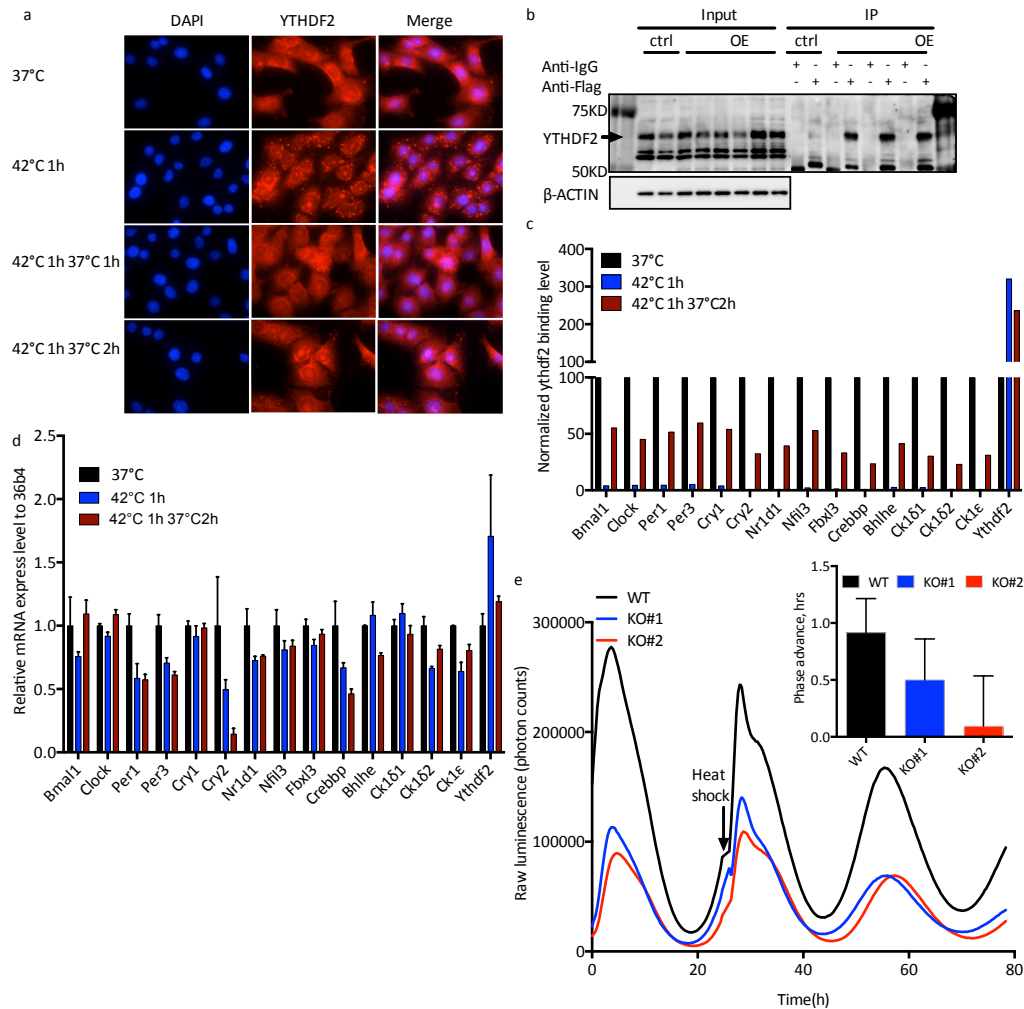
Figure 6. YTHDF2 relocates to stress granules under heat shock.

(**a**) PER2::LUC MEFs were immunostanied using the anti-YTHDF2 antibody under normal conditions or after heat shock (42°C, 1h), and recovery at 37°C for 1 or 2 hours. DAPI was used for nuclear counterstaining. Representative pictures of at least three independent experiments. (**b**) Lysates from PER2::LUC transfected with FLAG-YTHDF2 or the empty vecor were prepared for RNA-binding protein immunoprecipitation (RIP) with the anti-FLAG antibody, and FLAG-YTHDF2 IP was confirmed using the anti-YTHDF2 antibody. Mouse IgG was used as a negative control for RIP. (**c**) Decrease in binding of clock-related transcripts to FLAG-YTHDF2 after heat shock, and partial recovery after 2h at 37°C post heat shock, identified by FLAG-YTHDF2 RIP combined with RT-qPCR. (**d**) Heat shock does not affect the expression level of YTHDF2 sensitive transcripts, identified by RT-qPCR. (**e**) A one-hour heat shock 4 hours after the trough of PER2::LUC caused an ~1 hour phase advance in wild-type cells, but *Ythdf2* KO seem to blunt this resetting response. Period resetting was analyzed by student *t*-test, but no significance was detected. Data are shown mean ± SEM, n = 2 for WT and 3 for KO#1 and KO#2.

70

REFERENCES

[1] J.A. Mohawk, C.B. Green, J.S. Takahashi. Central and peripheral circadian clocks in mammals. Annu Rev Neurosci, 35 (**2012**) 445-462.

[2] F.K. Stephan, I. Zucker. Circadian rhythms in drinking behavior and locomotor activity of rats are eliminated by hypothalamic lesions. Proc Natl Acad Sci U S A, 69 (**1972**) 1583-1586.

[3] J.A. Mohawk, J.S. Takahashi. Cell autonomy and synchrony of suprachiasmatic nucleus circadian oscillators. Trends Neurosci, 34 (**2011**) 349-358.

[4] J.S. Takahashi. Transcriptional architecture of the mammalian circadian clock. Nat Rev Genet, 18 (**2017**) 164-179.

[5] Y. Fu, D. Dominissini, G. Rechavi, C. He. Gene expression regulation mediated through reversible m(6)A RNA methylation. Nat Rev Genet, 15 (**2014**) 293-306.

[6] I.U. Haussmann, Z. Bodi, E. Sanchez-Moran, N.P. Mongan, N. Archer, R.G. Fray, M. Soller. m6A potentiates Sxl alternative pre-mRNA splicing for robust Drosophila sex determination. Nature, 540 (**2016**) 301-304.

[7] H. Huang, H. Weng, W. Sun, X. Qin, H. Shi, H. Wu, . . . J. Chen. Recognition of RNA N(6)-methyladenosine by IGF2BP proteins enhances mRNA stability and translation. Nat Cell Biol, 20 (**2018**) 285-295.

[8] J.M. Fustin, R. Kojima, K. Itoh, H.Y. Chang, S. Ye, B. Zhuang, . . . H. Okamura. Two Ck1delta transcripts regulated by m6A methylation code for two antagonistic kinases in the control of the circadian clock. Proc Natl Acad Sci U S A, 115 (**2018**) 5980-5985.

[9] H. Shi, X. Wang, Z. Lu, B.S. Zhao, H. Ma, P.J. Hsu, . . . C. He. YTHDF3 facilitates translation and decay of N6-methyladenosine-modified RNA. Cell Res, 27 (**2017**) 315-328.

[10] X. Wang, B.S. Zhao, I.A. Roundtree, Z. Lu, D. Han, H. Ma, . . . C. He. N(6)-methyladenosine modulates messenger RNA translation efficiency. Cell, 161 (**2015**) 1388-1399.

[11] T. Glisovic, J.L. Bachorik, J. Yong, G. Dreyfuss. RNA-binding proteins and post-transcriptional gene regulation. FEBS Lett, 582 (**2008**) 1977-1986.

[12] X. Wang, Z. Lu, A. Gomez, G.C. Hon, Y. Yue, D. Han, . . . C. He. N6-methyladenosine-dependent regulation of messenger RNA stability. Nature, 505 (**2014**) 117-120.

[13] B.S. Zhao, X. Wang, A.V. Beadell, Z. Lu, H. Shi, A. Kuuspalu, . . . C. He. m6A-dependent maternal mRNA clearance facilitates zebrafish maternal-to-zygotic transition. Nature, 542 (**2017**) 475-478.

[14] I. Ivanova, C. Much, M. Di Giacomo, C. Azzi, M. Morgan, P.N. Moreira, . . . D. O'Carroll. The RNA m(6)A reader YTHDF2 is essential for the post-transcriptional regulation of the maternal transcriptome and oocyte competence. Mol Cell, 67 (**2017**) 1059-1067.

[15] M.J. Son, W.K. Kim, K.J. Oh, A. Park, S. Lee da, B.S. Han, . . . K.H. Bae. Methyltransferase and demethylase profiling studies during brown adipocyte

differentiation. BMB Rep, 49 (**2016**) 388-393.

[16] T. Lence, J. Akhtar, M. Bayer, K. Schmid, L. Spindler, C.H. Ho, . . . J.Y. Roignant. m6A modulates neuronal functions and sex determination in Drosophila. Nature, 540 (**2016**) 242-247.

[17] H. Shi, X. Zhang, Y.L. Weng, Z. Lu, Y. Liu, Z. Lu, . . . T. Zhou. m(6)A facilitates hippocampus-dependent learning and memory through YTHDF1. Nature, 563 (**2018**) 249-253.

[18] G. Lichinchi, B.S. Zhao, Y. Wu, Z. Lu, Y. Qin, C. He, T.M. Rana. Dynamics of human and viral RNA methylation during zika virus infection. Cell Host Microbe, 20 (**2016**) 666-673.

[19] G. Lichinchi, S. Gao, Y. Saletore, G.M. Gonzalez, V. Bansal, Y. Wang, . . . T.M. Rana. Dynamics of the human and viral m(6)A RNA methylomes during HIV-1 infection of T cells. Nat Microbiol, 1 (**2016**) 16011.

[20] Q. Cui, H. Shi, P. Ye, L. Li, Q. Qu, G. Sun, . . . Y. Shi. m(6)A RNA Methylation Regulates the Self-Renewal and Tumorigenesis of Glioblastoma Stem Cells. Cell Rep, 18 (**2017**) 2622-2634.

[21] S. Lin, J. Choe, P. Du, R. Triboulet, Richard I. Gregory. The m6A Methyltransferase METTL3 Promotes Translation in Human Cancer Cells. Mol Cell, 62 (**2016**) 335-345.

[22] Y. Pan, P. Ma, Y. Liu, W. Li, Y. Shu. Multiple functions of m(6)A RNA methylation in cancer. J Hematol Oncol, 11 (**2018**) 48.

[23] Z.X. Liu, L.M. Li, H.L. Sun, S.M. Liu. Link between m6A modification and cancers. Front Bioeng Biotechnol, 6 (**2018**) 89.

[24] J. Liu, M.A. Eckert, B.T. Harada, S.M. Liu, Z. Lu, K. Yu, . . . C. He. m(6)A mRNA methylation regulates AKT activity to promote the proliferation and tumorigenicity of endometrial cancer. Nat Cell Biol, 20 (**2018**) 1074-1083.

[25] K.D. Meyer, S.R. Jaffrey. The dynamic epitranscriptome: N6-methyladenosine and gene expression control. Nat Rev Mol Cell Biol, 15 (**2014**) 313-326.

[26] J.A. Bokar, M.E. Shambaugh, D. Polayes, A.G. Matera, F.M. Rottman. Purification and cDNA cloning of the AdoMet-binding subunit of the human mRNA (N6-adenosine)-methyltransferase. RNA, 3 (**1997**) 1233-1247.

[27] J. Liu, Y. Yue, D. Han, X. Wang, Y. Fu, L. Zhang, . . . C. He. A METTL3-METTL14 complex mediates mammalian nuclear RNA N6-adenosine methylation. Nat Chem Biol, 10 (**2014**) 93-95.

[28] X.L. Ping, B.F. Sun, L. Wang, W. Xiao, X. Yang, W.J. Wang, . . . Y.G. Yang. Mammalian WTAP is a regulatory subunit of the RNA N6-methyladenosine methyltransferase. Cell Res, 24 (**2014**) 177-189.

[29] G. Zheng, J.A. Dahl, Y. Niu, P. Fedorcsak, C.M. Huang, C.J. Li, . . . C. He. ALKBH5 is a mammalian RNA demethylase that impacts RNA metabolism and mouse fertility. Mol Cell, 49 (**2013**) 18-29.

[30] G. Jia, Y. Fu, X. Zhao, Q. Dai, G. Zheng, Y. Yang, . . . C. He. N6-methyladenosine in nuclear RNA is a major substrate of the obesity-associated FTO. Nat Chem Biol, 7

(**2011**) 885-887.

[31] N. Liu, Q. Dai, G. Zheng, C. He, M. Parisien, T. Pan. N(6)-methyladenosine-dependent RNA structural switches regulate RNA-protein interactions. Nature, 518 (**2015**) 560-564.

[32] N. Liu, K.I. Zhou, M. Parisien, Q. Dai, L. Diatchenko, T. Pan. N6-methyladenosine alters RNA structure to regulate binding of a low-complexity protein. Nucleic Acids Res, 45 (**2017**) 6051-6063.

[33] C.R. Alarcon, H. Goodarzi, H. Lee, X. Liu, S. Tavazoie, S.F. Tavazoie. HNRNPA2B1 Is a Mediator of m(6)A-Dependent Nuclear RNA Processing Events. Cell, 162 (**2015**) 1299-1308.

[34] P.J. Hsu, Y. Zhu, H. Ma, Y. Guo, X. Shi, Y. Liu, . . . C. He. Ythdc2 is an N6-methyladenosine binding protein that regulates mammalian spermatogenesis. Cell Res, 27 (**2017**) 1115-1127.

[35] F. Li, D. Zhao, J. Wu, Y. Shi. Structure of the YTH domain of human YTHDF2 in complex with an m(6)A mononucleotide reveals an aromatic cage for m(6)A recognition. Cell Res, 24 (**2014**) 1490-1492.

[36] D. Dominissini, S. Moshitch-Moshkovitz, S. Schwartz, M. Salmon-Divon, L. Ungar, S. Osenberg, . . . G. Rechavi. Topology of the human and mouse m6A RNA methylomes revealed by m6A-seq. Nature, 485 (**2012**) 201-206.

[37] J. Chen, Y. Sun, X. Xu, D. Wang, J. He, H. Zhou, . . . M. Xu. YTH domain family 2 orchestrates epithelial-mesenchymal transition/proliferation dichotomy in pancreatic cancer cells. Cell Cycle, 16 (**2017**) 2259-2271.

[38] H. Du, Y. Zhao, J. He, Y. Zhang, H. Xi, M. Liu, . . . L. Wu. YTHDF2 destabilizes m(6)A-containing RNA through direct recruitment of the CCR4-NOT deadenylase complex. Nat Commun, 7 (**2016**) 12626.

[39] S. Rauch, C. He, B.C. Dickinson. Targeted m(6)A Reader Proteins To Study Epitranscriptomic Regulation of Single RNAs. J Am Chem Soc, 140 (**2018**) 11974-11981.

[40] J. Zhou, J. Wan, X. Gao, X. Zhang, S.R. Jaffrey, S.B. Qian. Dynamic m(6)A mRNA methylation directs translational control of heat shock response. Nature, 526 (**2015**) 591-594.

[41] J. Mauer, X. Luo, A. Blanjoie, X. Jiao, A.V. Grozhik, D.P. Patil, . . . S.R. Jaffrey. Reversible methylation of m6Am in the 5' cap controls mRNA stability. Nature, 541 (**2017**) 371-375.

[42] M. Cardelli, F. Marchegiani, L. Cavallone, F. Olivieri, S. Giovagnetti, E. Mugianesi, . . . C. Franceschi. A Polymorphism of the YTHDF2 Gene (1p35) Located in an Alu-Rich Genomic Domain Is Associated With Human Longevity. J Gerontol, 61 (**2006**) 547-556.

[43] F.A. Ran, P.D. Hsu, J. Wright, V. Agarwala, D.A. Scott, F. Zhang. Genome engineering using the CRISPR-Cas9 system. Nat Protoc, 8 (**2013**) 2281-2308.

[44] A. Dobin, C.A. Davis, F. Schlesinger, J. Drenkow, C. Zaleski, S. Jha, . . . T.R. Gingeras. STAR: ultrafast universal RNA-seq aligner. Bioinformatics, 29 (**2012**) 15-21.

[45] M. Pertea, D. Kim, G.M. Pertea, J.T. Leek, S.L. Salzberg. Transcript-level expression analysis of RNA-seq experiments with HISAT, StringTie and Ballgown. Nat Protoc, 11 (**2016**) 1650-1667.

[46] M. Pertea, G.M. Pertea, C.M. Antonescu, T.C. Chang, J.T. Mendell, S.L. Salzberg. StringTie enables improved reconstruction of a transcriptome from RNA-seq reads. Nat Biotechnol, 33 (**2015**) 290-295.

[47] Z. Li, P. Qian, W. Shao, H. Shi, X.C. He, M. Gogol, . . . L. Li. Suppression of m(6)A reader Ythdf2 promotes hematopoietic stem cell expansion. Cell Res, 28 (**2018**) 904-917.

[48] M. Li, X. Zhao, W. Wang, H. Shi, Q. Pan, Z. Lu, . . . A. Klungland. Ythdf2-mediated m(6)A mRNA clearance modulates neural development in mice. Genome Biol, 19 (**2018**) 69.

[49] D.P. Patil, C.K. Chen, B.F. Pickering, A. Chow, C. Jackson, M. Guttman, S.R. Jaffrey. m(6)A RNA methylation promotes XIST-mediated transcriptional repression. Nature, 537 (**2016**) 369-373.

[50] N.S. Gokhale, A.B.R. McIntyre, M.J. McFadden, A.E. Roder, E.M. Kennedy, J.A. Gandara, . . . S.M. Horner. N6-Methyladenosine in Flaviviridae Viral RNA Genomes Regulates Infection. Cell Host Microbe, 20 (**2016**) 654-665.

[51] E.M. Kennedy, H.P. Bogerd, A.V. Kornepati, D. Kang, D. Ghoshal, J.B. Marshall, . . . B.R. Cullen. Posttranscriptional m(6)A Editing of HIV-1 mRNAs Enhances Viral Gene Expression. Cell Host Microbe, 19 (**2016**) 675-685.

[52] S. Schwartz, M.R. Mumbach, M. Jovanovic, T. Wang, K. Maciag, G.G. Bushkin, . . . A. Regev. Perturbation of m6A writers reveals two distinct classes of mRNA methylation at internal and 5' sites. Cell Rep, 8 (**2014**) 284-296.

[53] T. Tamaru, M. Hattori, K. Honda, I. Benjamin, T. Ozawa, K. Takamatsu. Synchronization of circadian Per2 rhythms and HSF1-BMAL1:CLOCK interaction in mouse fibroblasts after short-term heat shock pulse. PloS one, 6 (**2011**) e24521.

[54] A. Sandqvist, L. Sistonen. Nuclear stress granules. J Cell Biol, 164 (**2004**) 15.

[55] J.M. Fustin, M. Doi, Y. Yamaguchi, H. Hida, S. Nishimura, M. Yoshida, . . . H. Okamura. RNA-methylation-dependent RNA processing controls the speed of the circadian clock. Cell, 155 (**2013**) 793-806.

[56] R. Narasimamurthy, S.R. Hunt, Y. Lu, J.M. Fustin, H. Okamura, C.L. Partch, . . . D.M. Virshup. CK1delta/epsilon protein kinase primes the PER2 circadian phosphoswitch. Proc Natl Acad Sci U S A, 115 (**2018**) 5986-5991.

[57] R.J. Ries, S. Zaccara, P. Klein, A. Olarerin-George, S. Namkoong, B.F. Pickering, . . . S.R. Jaffrey. m6A enhances the phase separation potential of mRNA. Nature, 571 (**2019**) 424-428.

[58] D.S.W. Protter, R. Parker. Principles and properties of stress granules. Trends Cell Biol, 26 (**2016**) 668-679.

CHAPTER 3

TWO CK1δ TRANSCRIPTS REGULATED BY m6A METHYLATION CODE FOR TWO ANTAGONISTIC KINASES IN THE CONTROL OF THE CIRCADIAN CLOCK

ABSTRACT

Over 150 RNA modifications have been identified as the foundation of "RNA epigenetics", with N^6-methyladenosine (m6A) in mRNAs being the most abundant and the best studied. Firstly discovered in 1974, m6A has been shown to affect mRNA stability, splicing, export and translation, highlighting its role in gene regulation, animal development and human diseases. m6A has been quantified on many clock gene transcripts and related regulators, such as *Ck1δ* mRNA, and the inhibition of m6A methylation by silencing the m6A writer *Mettl3* is sufficient to cause circadian period elongation. Moreover, m6A negatively regulates the expression of two novel alternatively spliced *Ck1δ* isoforms, *Ck1δ1* and *Ck1δ2*. However, the relative expression of these two isoforms is tissue-specific but the mechanisms underlying this regulation are unknown. Here, by using *in vitro* translation and transcription, I demonstrate that the common 3'-UTR of the *Ck1δ* isoforms is a negative regulator of translation, and that the 63 bp *Ck1δ2*-specific exon by itself determines the different half-life of *Ck1δ1* and *Ck1δ2* mRNAs. These discoveries help to understand how *Ck1δ* isoforms are regulated.

INTRODUCTION

In RNA epigenetics, m6A is the most prevalent internal RNA modification, existing in 0.1–0.4% of all adenosines in whole cellular RNAs [1]. Only until recent years, its potential functional significance and extent transcript identities have been gradually elucidated. With the advancement of m6A immunoprecipitation coupled with RNA-sequencing, m6A has been shown to occur primarily in two consensus sequence

motifs, G m6A C (~70%) and A m6A C (~30%) [2, 3]. Moreover, long internal exons, locus near the upstream of stop codons, and in particular, the 3'-UTR of mRNA are preferred m6A modification locus [4], in coincidence with its roles involving RNA stability, splicing, export and translation .

The circadian clock is controlled by transcription-translation negative feedback loops (TTFL) that regulate the oscillation of clock genes that are composed of the activators Clock and its heterodimeric partner BMAL1, and the repressors PER1-3 and CRY1-2 [5]. The TTFL-controlled circadian clock is sensitive to inputs affecting gene transcription, RNA processing and protein modification. While the core TTFL has been the focus of early circadian research, protein phosphorylation was quickly shown to be essential for molecular timekeeping [6, 7]. Phosphorylation of the clock protein PER2 is mediated mainly by the casein kinases 1 Delta (CK1δ) and casein kinases 1 Epsilon [8]. The first human inherited circadian syndrome to be described, the Familial Advanced Sleep Phase Syndrome (FASPS), originates from a mutated CK1δ [9] or a mutated CK1δ-target serine in the PER2 protein [10], causing early sleep onset and offset.

Recently, through investigation of m6A RNA sequencing data, the 3'-UTR of the *Ck1δ* mRNAs was been found to be heavily methylated, suggesting the regulatory role of m6A on *Ck1δ* and its relationship on circadian clock. Interestingly, our lab later identified the two bands as two isoforms of CK1δ, CK1δ1 (415 aa) and CK1δ2 (409 aa), sharing 99.75% identity with human CK1δs, and conserved in virtually all vertebrates. The only difference between mRNAs of these isoforms is a small 63-bp exon in mouse, retained in the *Ck1δ2 mRNA* immediately upstream of the 3'-UTR and containing a STOP codon, thus coding for the smaller kinase. While CK1δ1 accelerates the circadian clock by promoting the decay of the PER2 protein, CK1δ2 slows it down by stabilizing PER2 via increased phosphorylation at a key residue on the PER2 protein. These observations challenge the previously established model of PER2 phosphorylation and, given the multiple functions and targets of CK1δ, the

existence of two isoforms calls for a re-evaluation of past research when CK1δ1 and CK1δ2 were simply CK1δ.

Surprisingly, the half-life of *Ck1δ2* was significantly longer than that of *Ck1δ1*, which we confirmed in a longer time course. Upon mRNA m6A inhibition, silencing of *Mettl3* increased the intensity of the two bands, demonstrating m6A negatively regulates CK1δ expression. However, the underlying mechanism of the divergence of these two isoforms remain unknow, especially its relationship with highly methylated 3'-UTR region and whole m6A status. Here, I investigate the influence of 3'-UTR region and m6A modification on stability and translation of the CK1δ1 and CK1δ2 mRNAs.

METHODS AND MATERIALS

In vitro transcription

The promoter and 5' UTR of *Ck1δ* was cloned into a pGL4.12 backbone (Promega) upstream of the destabilized luciferase LUC2CP coding sequence, and the 3'-end of the *Ck1δ1* or *Ck1δ2* coding sequences, followed by their respective 3'-UTRs, were cloned downstream of the LUC2CP STOP codon. Partial deletion of the 3'-UTR in the vectors was achieved by conventional sequential PCR rounds to truncate the 3'-UTR region between the native NsiI and MfeI restriction sites. Essentially, the 5'-GATCTACTCTGTTACCAATG-3' upstream sequence in the 3'-UTR was joined to the 5'-ACTAGGACCATTGGAAGTCC-3' downstream. Linear templates for *in vitro* transcription were then amplified by PCR, with the 5'-<u>TAATACGACTCACTATAGGG</u>AGAAGTGACGTCACAGCGCGATGGCGG-3' forward and 5'-GAGGGAAGAAAGGTAGAAGTCATTATG-3' reverse primer. The forward primer contained a T7 promoter overhang (underlined) for *in vitro* transcription. Messenger RNAs were transcribed *in vitro* using the mMESSENGER mMACHINE T7 ULTRA kit (Invitrogen) following manufacturer's protocol with or without 20% m6ATP/ATP (Trilink Biotechnologies) added to the mix where appropriate. A control mRNA

containing the Renilla luciferase coding sequence was also *in vitro* transcribed (without m6ATP) from the pRL-SV40 linearized vector (Promega). To confirm specificity of transcription, all mRNAs were checked by denaturing agarose gel electrophoresis.

In vitro translation

The Flexi Rabbit Reticulocyte Lysate System (Promega) was used following manufacturer's instructions with the following modifications. Wild-type MEFs in 24 well plates were then transfected with the appropriate *Ck1δ* mRNA and the *Renilla* control mRNA (1000:1) using MessengerMAX lipofectamine (Invitrogen) following the product manual in medium containing 1 mM luciferin or 30 ug/ml Enduren (Promega), and immediately transferred to a real-time luminometer-incubator (CL24A-LIC, Churitsu), counting each well for 10 seconds at 10 min intervals.

RESULTS

The 3'-UTR is a negative regulator of CK1δ translation

The 3'-UTR of *Ck1δ* transcripts is over 2,000 nucleotides long, but its function in the regulation of CK1δ expression is unknown. I designed reporter mRNAs in which the luciferase coding sequence was flanked by the 5'- and 3'-UTRs of *Ck1δ*. To closely mimic *Ck1δ1* and *Ck1δ2*, the end of the coding sequence of each *Ck1δ* was also included downstream of the luciferase STOP codon. I also designed *Ck1δluc* transcripts lacking most of the 3'-UTR (Fig. 1a, b). These reporter mRNAs were transcribed *in vitro* and then added to reticulocyte lysates to assess the efficiency of their translation by luminometry, together with a control mRNA coding for *Renilla luciferase*. Endpoint luminescence was then quantified, showing that deletion of the 3'-UTR caused a significant increase in CK1δ1LUC (approximately six folds) and CK1δ2LUC (approximately threefold) luminescence, demonstrating the role of the 3'-UTR as a negative regulator of CK1δ translation (Fig. 1c).

<u>Two *Ck1δ* alternative transcripts are under m6A control</u>

To investigate the role of the methylation of *Ck1δ* mRNA on processing and translation dynamically, full length *Ck1δluc* reporter mRNAs, transcribed *in vitro* with or without 20% m6ATP/ATP, were transfected into wild-type mouse embryonic fibroblasts (MEFs) together with *Renilla* control mRNA. Luminescence from Photinus and Renilla luciferases were then followed in real-time from the beginning of transfection. Since I provided the cells with a limited amount of transcripts, the rise and fall in reporter activity mirrored both translation efficiency and mRNA decay, which have been shown to be both facilitated by m6A. Indeed, incorporation of m6A into the mRNAs accelerated the dynamics (earlier rise of reporter activity to peak values and faster decay from the peak) of both reporter transcripts (Fig. 1d).

DISCUSSION

From the *in vitro* transcription-translation assay shown here, the presence of m6A within *Ck1δlucUTR* transcripts as expected promoted more dynamic mRNA processing. It should be mentioned however that the incorporation of m6A in these experiments was random, while the location of the m6A site in endogenous *Ck1δ* transcripts is very specifically in the 3'-UTR, at a canonical GGACA sequence 171 or 252 nucleotides downstream of the STOP codon in *Ck1δ1* or *Ck1δ2*, respectively.

To more precisely investigate the effect of m6A methylation on the regulation of *Ck1δ* transcripts, it would be very interesting to be able to reproduce *in vitro* the m6A-methylation pattern of *in vivo* transcripts. A solution would be to incubate *in vitro*-transcribed mRNA with nuclear extracts from Hela cells (for example ABCAM ab150036), which express high levels of the m6A writer METTL3, and have been used extensively in m6A research [11]. The presence of the m6A writer complex in these nuclear extracts may lead to position-specific N^6-adenosyl methylation of the *in*

vitro-transcribed mRNA, which coud then be purified via antisense-oligo coupled to magnetic beads. This will be tested in the future to continue these experiments.
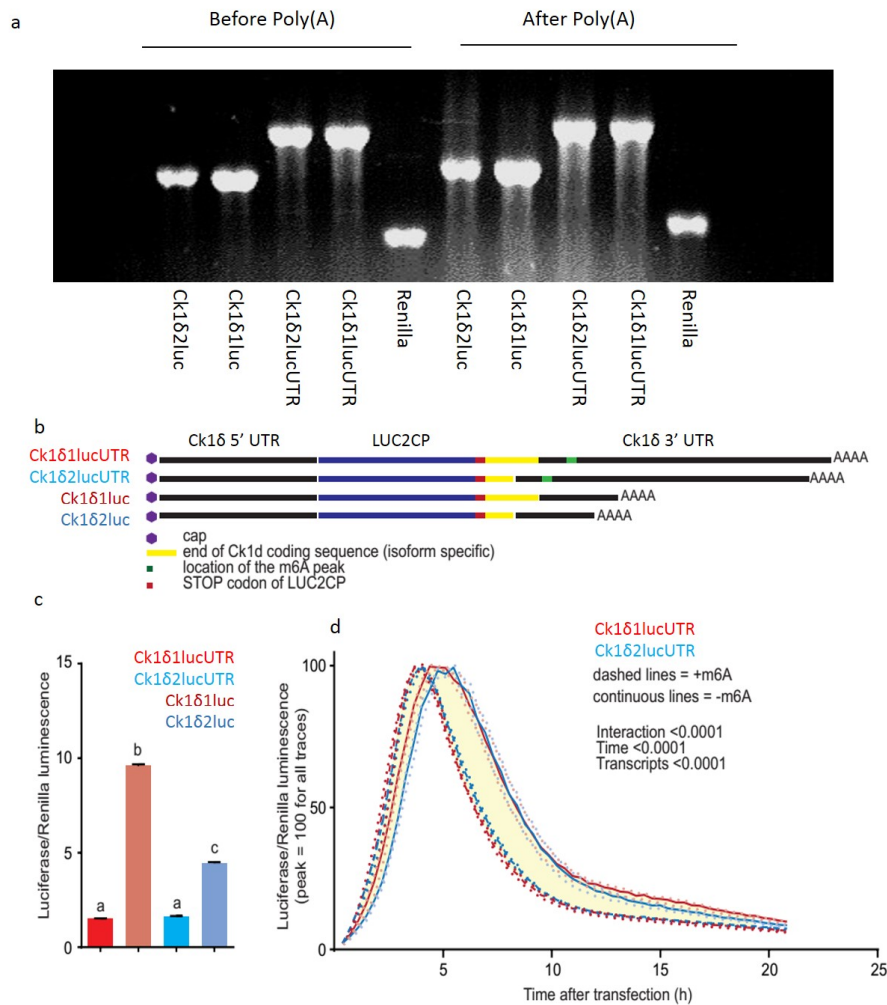

Figure 1. Two CK1δ alternative transcripts are under m6A control and the 3'-UTR is a negative regulator of translation. a, Denaturing agarose gel electrophoresis of *in vitro* transcribed mRNA, before and after polyadenylation. b, The schema shows the structure of each reporter transcript. *In vitro* transcription of *Ck1δ*-like luciferase reporter mRNAs followed by *in vitro* translation (c), or transfection in MEFs (d). Analyzed by One-Way ANOVA, *p* <0.0001; a, b, c labels indicate *p* <0.0001 significance in Bonferroni post-hoc analysis, n=4. (d) Full length mRNAs show faster dynamics of translation and turnover when methylated. Data were analyzed by Two-Way ANOVA followed by Bonferroni post-hoc, n=3. The areas between the

traces highlighted in pale yellow indicate at least p <0.05 significance in Bonferroni post-hoc. Data shown are mean +/- SEM.

REFERENCES

[1] C. Zhang, J. Fu, Y. Zhou. A Review in Research Progress Concerning m6A Methylation and Immunoregulation. Front Immunol, 10 (2019) 922.

[2] C.M. Wei, A. Gershowitz, B. Moss. 5'-Terminal and internal methylated nucleotide sequences in HeLa cell mRNA. Biochemistry, 15 (1976) 397-401.

[3] C.-M. Wei, B. Moss. Nucleotide sequences at the N6-methyladenosine sites of HeLa cell messenger ribonucleic acid. Biochemistry, 16 (1977) 1672-1676.

[4] K.D. Meyer, Y. Saletore, P. Zumbo, O. Elemento, C.E. Mason, S.R. Jaffrey. Comprehensive analysis of mRNA methylation reveals enrichment in 3' UTRs and near stop codons. Cell, 149 (2012) 1635-1646.

[5] J.S. Takahashi. Transcriptional architecture of the mammalian circadian clock. Nat Rev Genet, 18 (2017) 164-179.

[6] J.L. Price, J. Blau, A. Rothenfluh, M. Abodeely, B. Kloss, M.W. Young. double-time Is a Novel Drosophila Clock Gene that Regulates PERIOD Protein Accumulation. Cell, 94 (1998) 83-95.

[7] P.L. Lowrey, K. Shimomura, M.P. Antoch, S. Yamazaki, P.D. Zemenides, M.R. Ralph, . . . J.S. Takahashi. Positional syntenic cloning and functional characterization of the mammalian circadian mutation tau. Science, 288 (2000) 483-492.

[8] K. Vanselow, J.T. Vanselow, P.O. Westermark, S. Reischl, B. Maier, T. Korte, . . . A. Kramer. Differential effects of PER2 phosphorylation: molecular basis for the human familial advanced sleep phase syndrome (FASPS). Genes Dev, 20 (2006) 2660-2672.

[9] Y. Xu, Q.S. Padiath, R.E. Shapiro, C.R. Jones, S.C. Wu, N. Saigoh, . . . Y.-H. Fu. Functional consequences of a CKIδ mutation causing familial advanced sleep phase syndrome. Nature, 434 (2005) 640-644.

[10] K.L. Toh, C.R. Jones, Y. He, E.J. Eide, W.A. Hinz, D.M. Virshup, . . . Y.H. Fu. An hPer2 phosphorylation site mutation in familial advanced sleep phase syndrome. Science, 291 (2001) 1040-1043.

[11] J. Choe, S. Lin, W. Zhang, Q. Liu, L. Wang, J. Ramirez-Moya, . . . R.I. Gregory. mRNA circularization by METTL3-eIF3h enhances translation and promotes oncogenesis. Nature, 561 (2018) 556-560.

ACKNOWLEDGEMENTS